JAEA-Review
2008-008

Review of JAEA Activities on the IFMIF Liquid Lithium Target in FY2006

Mizuho IDA, Hiroo NAKAMURA, Teruo CHIDA*, Makoto MIYASHITA
Kazuyuki FURUYA*, Eiichi YOSHIDA, Yasushi HIRAKAWA, Osamu MIYAKE
Masaru HIRABAYASHI, Kuniaki ARA and Masayoshi SUGIMOTO

IFMIF Development Group
Fusion Research and Development Directorate

March 2008
Japan Atomic Energy Agency
日本原子力研究開発機構

JAEA-Review

本レポートは日本原子力研究開発機構が不定期に発行する成果報告書です。
本レポートの入手並びに著作権利用に関するお問い合わせは、下記あてにお問い合わせ下さい。
なお、本レポートの全文は日本原子力研究開発機構ホームページ（http://www.jaea.go.jp/index.shtml）より発信されています。このほか財団法人原子力弘済会資料センター*では実費による複写頒布を行っております。

〒319-1195　茨城県那珂郡東海村白方白根 2 番地 4
日本原子力研究開発機構　研究技術情報部　研究技術情報課
電話 029-282-6387, Fax 029-282-5920

*〒319-1195　茨城県那珂郡東海村白方白根 2 番地 4　日本原子力研究開発機構内

This report is issued irregularly by Japan Atomic Energy Agency
Inquiries about availability and/or copyright of this report should be addressed to
Intellectual Resources Section, Intellectual Resources Department,
Japan Atomic Energy Agency
2-4 Shirakata Shirane, Tokai-mura, Naka-gun, Ibaraki-ken 319-1195 Japan
Tel +81-29-282-6387, Fax　+81-29-282-5920

Review of JAEA Activities on the IFMIF Liquid Lithium Target in FY2006

Mizuho IDA[※1], Hiroo NAKAMURA, Teruo CHIDA[＊1], Makoto MIYASHITA[※1], Kazuyuki FURUYA[＊2]
Eiichi YOSHIDA[＋1], Yasushi HIRAKAWA[＋1], Osamu MIYAKE[＋1], Masaru HIRABAYASHI[＋2]
Kuniaki ARA[＋2] and Masayoshi SUGIMOTO[＋3]

Rokkasho BA Project Unit
Fusion Research and Development Directorate
Japan Atomic Energy Agency
Naka-shi, Ibaraki-ken

(Received January 16, 2008)

Engineering Validation Design and Engineering Design Activity (EVEDA) of the International Fusion Materials Irradiation Facility (IFMIF) is under going. IFMIF is an accelerator-based Deuterium-Lithium (D-Li) neutron source to produce intense high energy neutrons and a sufficient irradiation volume for testing candidate materials for fusion reactors. To realize such a condition, 40 MeV deuteron beam with a current of 250 mA is injected into high speed liquid Li flow with a speed of 20 m/s. In target system, nuclear heating due to neutron causes thermal stress especially on a back-wall of the target assembly. In addition, radioactive species such as beryllium-7, tritium and activated corrosion products are generated. In this report, thermal stress analyses of the back-wall, mechanical tests on weld specimen made of the back-wall material, estimations of beryllium-7 behavior and worker dose at the IFMIF Li loop and consideration on major EVEDA tasks are summarized.

Keywords: IFMIF, Lithium Target, Nuclear Heating, Thermal Stress, Beryllium-7, Worker Dose, EVEDA, Lithium Safety

---

＋1 Technology Development Department, Oarai Research and Development Center
＋2 FBR System Technology Development Unit, Advanced Nuclear System Research and Development Directorate
＋3 Fusion Research and Development Directorate
※1 Collaborating Engineer
＊1 Hitachi Engineering & Services Co., Ltd.
＊2 Hachinohe National College of Technology

IFMIF液体リチウムターゲットに関する平成18年度の原子力機構の活動

日本原子力研究開発機構核融合研究開発部門
六ヶ所BAプロジェクトユニット
井田 瑞穂[※1]・中村 博雄・千田 輝夫[＊1]・宮下 誠[※1]・古谷 一幸[＊2]・吉田 英一[＋1]・平川 康[＋1]
三宅 収[＋1]・平林 勝[＋2]・荒 邦章[＋2]・杉本 昌義[＋3]

(2008年1月16日受理)

国際核融合材料照射施設(IFMIF)の工学実証・工学設計活動 (EVEDA)が実施中である。IFMIFは核融合炉材料の開発のための十分な照射体積を有する強力な加速器型中性子源である。このような中性子を発生させるために、最大エネルギー40 MeV、最大電流250 mAの重水素ビームを、最大流速20 m/sの液体リチウム流ターゲットに入射させる。ターゲット系では、中性子の核発熱によりターゲット背面壁に熱応力が発生する。さらに、ベリリウム-7をはじめとする放射性核種が発生する。本報告では、平成18年度の原子力機構におけるターゲット系の主要な活動として、核発熱条件下でのターゲット背面壁の熱応力解析、その材料の溶接後の機械特性の試験、リチウムループ内でのベリリウム-7挙動とそれによる作業員被曝の評価、および原子力機構を中心に実施予定の工学実証・工学設計タスクの検討結果を取りまとめた。

那珂核融合研究所（駐在）：〒311-0193 茨城県那珂市向山801-1
＋1 大洗研究開発センター技術開発部
＋2 次世代原子力システム研究開発部門FBR要素技術ユニット
＋3 核融合研究開発部門付
※1 技術開発協力員
＊1 （株）日立エンジニアリング・アンド・サービス
＊2 八戸工業高等専門学校

Contents

目次

1. Introduction

The International Fusion Materials Irradiation Facility (IFMIF) is an accelerator-based deuteron-lithium (D-Li) neutron source for testing the effects of neutron irradiation on the properties of candidate materials of fusion reactors. The IFMIF activity has been implemented since 1995 as an international collaboration under auspice of the International Energy Agency (IEA), and IFMIF design at 2003 was identified in IFMIF Comprehensive Design Report (CDR) [1.1]. The IFMIF activity is under going as the Engineering Validation and Engineering Design Activity (EVEDA) under a framework of the broader approach (BA) agreement enforced in 2007 by EU and Japan.

To provide the intense neutron flux of 4.5 x 10^{17} neutrons/m^2/s with a peak energy around 14 MeV (corresponding to damage rate up to 50 dpa/year), two deuteron beams with total current of 250 mA and energy of 40 MeV are injected into a flowing liquid lithium target, which is operated at maximum flow speed up to 20 m/s for removal of 10 MW heat deposition by the deuteron beams and suppression of the excessive increase of lithium temperature.

Toward engineering design of the target assembly which is a vessel to generate high-speed free-surface lithium flow, thermal stress in and deformation of the target assembly caused by nuclear heating during the IFMIF operation are key issues. Thermal stress analysis was performed using a calculation code and material data. Also preliminary mechanical tests on weld specimen made of the same materials as those used for the back-wall part of the target assembly were done. For safe operation of the IFMIF, radioactivity is one of key issues. Behavior of beryllium-7 (^{7}Be) in the Li loop and its effect upon worker dose was estimated using a calculation code, since its radioactivity is the most dominant among nuclides in the Li loop. For preparation of the start of EVEDA tasks, outlines of Li test loop construction/test and Li safety handling experiments were considered.

This report consists of the activities in FY2006 above mentioned, which were performed by Japan Atomic Energy Agency (JAEA).

Reference

[1.1] IFMIF International Team, "IFMIF Comprehensive Design Report", IEA on-line publication, http://www.iea.org/Textbase/techno/technologies/fusion/IFMIF-CDR_partA.pdf and partB.pdf

2. IFMIF Target Facility

2.1 Outline of Target Facility

The IFMIF mainly consists of the accelerator facility, the target facility and the test facilities. Features of IFMIF target are a lithium target for simulating fusion neutrons with energy peak around 14 MeV through D-Li reaction, and a liquid target for removal of heat locally deposited with high density inevitable at the high-flux neutron generation.

Three-dimensional arrangement of the target facility is shown in Fig. 2-1. Two deuteron beams with total current of 250 mA and energy of 40 MeV are injected into a rectangular foot-print of ^{H}50 mm x ^{W}200 mm on the lithium target. To remove this high heat load with density of 1 GW/m^2, the lithium target flows with flow velocity up to 20 m/s in the target assembly. The total heat load of 10 MW is removed through the heat removal system consisting of the primary lithium loop, the secondary organic-oil loop and the tertiary water loop. The primary lithium loop consists of a main loop with flow rate of 130 litter/s and a purification loop with impurity traps. Major design requirements are summarized in Table 2-1.

2.2 Target Assembly

Three-dimensional view of the target assembly is shown in Fig. 2-2. The target assembly with weight of about 600 kg is supported and adjusted by the support attached to both side walls of a Test Cell room under a condition of vacuum (1 x 10^{-3} Pa) or filled with Ar/He gas. The target assembly made of stainless steel 316 has lip seals (indicated in blue in Fig. 2-2) for welding/cutting by yttrium aluminum garnet (YAG) laser. Considering high irradiation damage up to 50 dpa/year, center part of the back-wall is made of reduced-activation ferritic/martensitic (RAFM) and replaced after every 11-months operation. There are two options for the replaceable back-wall. One is a back-wall with lip seal weld/cut as shown in Fig. 2-2. The other is a “bayonet type” back-wall with mechanical slide-guide and bolting. In the JAEA activity, the former type has been examined from viewpoint of thermal stress and deformation due to nuclear heating by neutrons during an operation.

Cross-sectional view of the target assembly is shown in Fig. 2-3. The liquid lithium with width of 260 mm flows down, with reducing its thickness from 250 mm to 25 mm and increasing its flow velocity up to 20 m/s in the double reducer nozzle, then along the concave back-wall with radium of 250 mm or more to avoid lithium boiling by a centrifugal force in the free-surface flow under the accelerator vacuum condition of 1 x 10^{-3} Pa. Surface behaviors of high-speed free-surface flow generated by a smaller double reducer nozzle have been experimentally examined under JAEA/Osaka University collaboration.

2.3 Lithium Loop

The function of the main lithium loop is removal of the heat up to 10 MW. As shown in Fig. 2-1, the main loop consists of an electro magnetic pump (EMP) to circulate the liquid lithium, the target assembly to form the liquid target, a quench tank to relax lithium temperature distribution localized due to the beam injection, a heat exchanger (HX) to cool the liquid lithium, and a dump tank to storage the lithium with inventory of 9 m^3. All components are made of 316 steel, excepting a RAFM for center part of the back-wall.

In the lithium loop, radioactive nuclides are produced through nuclear reaction between deuteron/neutron and lithium/steel elements. Radioactivity of corrosion products from an activated back-wall after 1year operation was estimated 4 x 10^{10} Bq.[2.1] Radioactivity of tritium remaining in the lithium loop was estimated 6 x 10^{14} Bq.[2.2] In comparison with them, radioactivity of beryllium-7 (^{7}Be) produced through ^{6}Li(D, n)^{7}Be and ^{7}Li(D, 2n)^{7}Be is larger (estimated 5 x 10^{15} Bq). Furthermore, a nuclide ^{7}Be decays emitting a gamma ray with high energy of 0.48 MeV, and sufficient reduction of the radioactivity within 1-month annual maintenance, since half-life of ^{7}Be is 53.3 days. Therefore, ^{7}Be is the most dominant nuclide from viewpoint of worker dose.[2.3] Effects of these radioactive nuclides have been estimated as JAEA activity.

Most of impurities including radioactive ones in liquid lithium are expected to be removed in the cold/hot traps in the lithium purification loop. Required concentration of each element is less than 10 wppm. Hydrogen isotopes (^{1}H, ^{2}H and ^{3}H) are trapped mainly in the hydrogen hot trap with yttrium (Y) sponge operated at 285 °C. Nitrogen are trapped mainly in the nitrogen hot trap operated at 600 °C or higher. Candidate materials for the nitrogen hot trap are vanadium titanium (V-Ti) alloy and zirconium (Zr).

References

[2.1] H. Nakamura, M. Takemura, M. Yamauchi, U. Fischer, M. Ida, S. Mori, T. Nishitani, S. Simakov and M. Sugimoto, “Accessibility Evaluation of the IFMIF Liquid Lithium Loop Considering Activated Erosion/Corrosion Materials Deposition”, Fusion Eng Des 75-79 (2005) pp.1169-1172.

[2.2] K. Matsuhiro, Hirofumi Nakamura, T. Hayashi, Hiroo Nakamura and M. Sugimoto, “Evaluation of Tritium Permeation from Lithium Loop of IFMIF Target System”, Fusion Science and Technology 48 (2005) pp.625-628.

[2.3] M. Ida, H. Nakamura T. Chida and M. Sugimoto, Review of JAEA Activities on the IFMIF Liquid Lithium Target in FY2005, JAEA report, JAEA-Review 2006-009 (2006).

Table 2-1 Major design requirements of IFMIF target facility.

Items	Parameters
Deuteron energy	40 MeV
Deuteron beam current	250 mA (125 mA x 2 accelerators)
Beam footprint on Li flow	^{H}50 mm x ^{W}200 mm
Beam power, heat flux	10 MW, 1 GW/m^2
Li flow thickness (inc. deviation), width	^{T}25±1 mm, ^{W}260 mm
Li flow average velocity	15 m/s (range: 10-20 m/s)
Li flow rate in main loop	0.13 m^3/s (at 20 m/s)
Nozzle geometry	Double reducer based on Shima's model
Nozzle contraction ratio	10 → 2.5 → 1 (^{T}250 → 62.5 → 25 mm)
Surface roughness of nozzle inner wall	< 6 μm
Li temperature at inlet	250 °C (nominal)
Vacuum condition at Li free surface	10^{-3} Pa
Vacuum, filling gas in Test Cell room	0.1 Pa, ~0.1 MPa-Ar/He (TBD)
Hydrogen isotopes concentration in Li	< 10 wppm (total of ^{1}H, ^{2}H, ^{3}H), < 1 wppm (^{3}H)
Impurity concentration in Li	< 10 wppm (each C, N, O)
Corrosion concentration in Li	TBD
Erosion/corrosion rate	< 1 μm/year (back-wall, nozzle)
	< 50 μm/30year (others)
Component material	RAF (center of the back-wall)
	316 steel (others, excepting impurity-getter materials)
Replacement period	Every 11-months operation (back-wall)
	No replacement in 30 years (others)
Alignment accuracy of back-wall	±0.5 mm
Availability of target facility	> 95 %

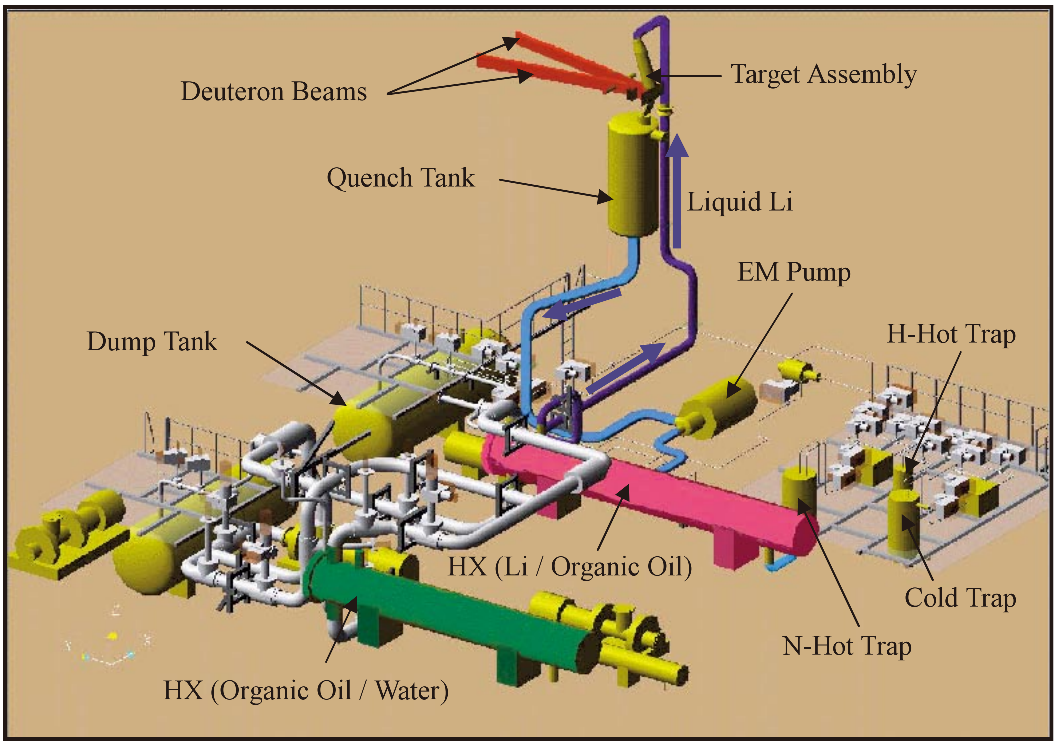

Fig. 2-1 Three-dimensional arrangement of the IFMIF target facility

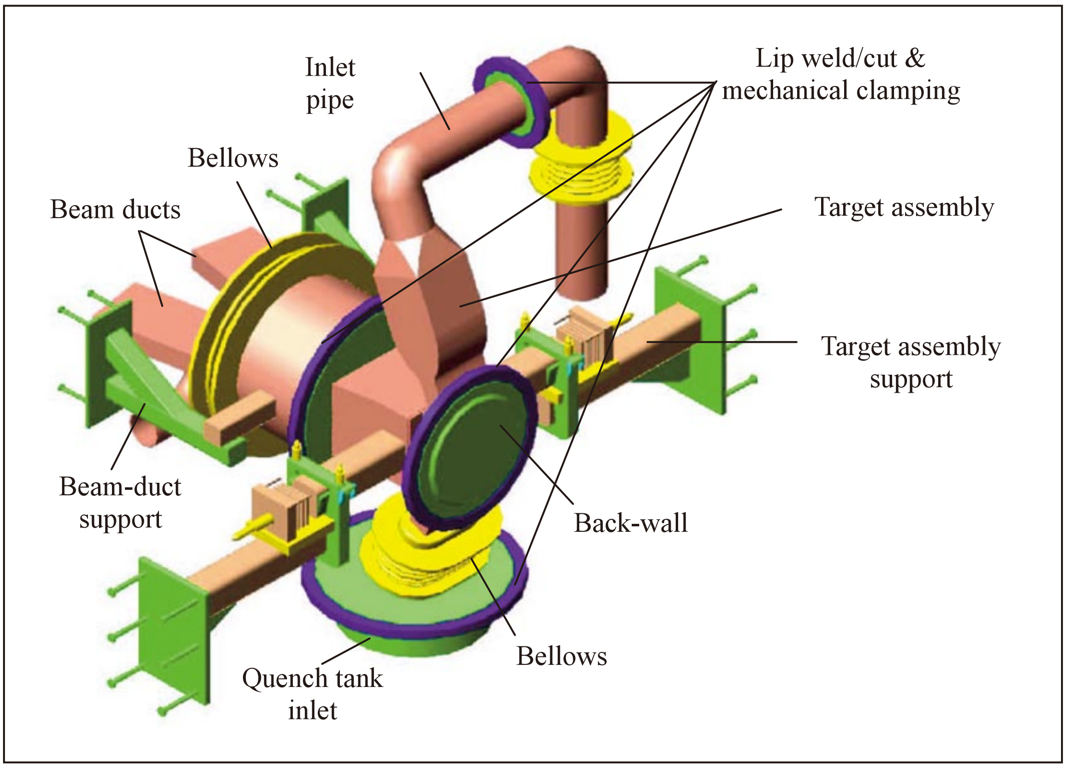

Fig. 2-2 Three-dimensional view of the IFMIF target assembly

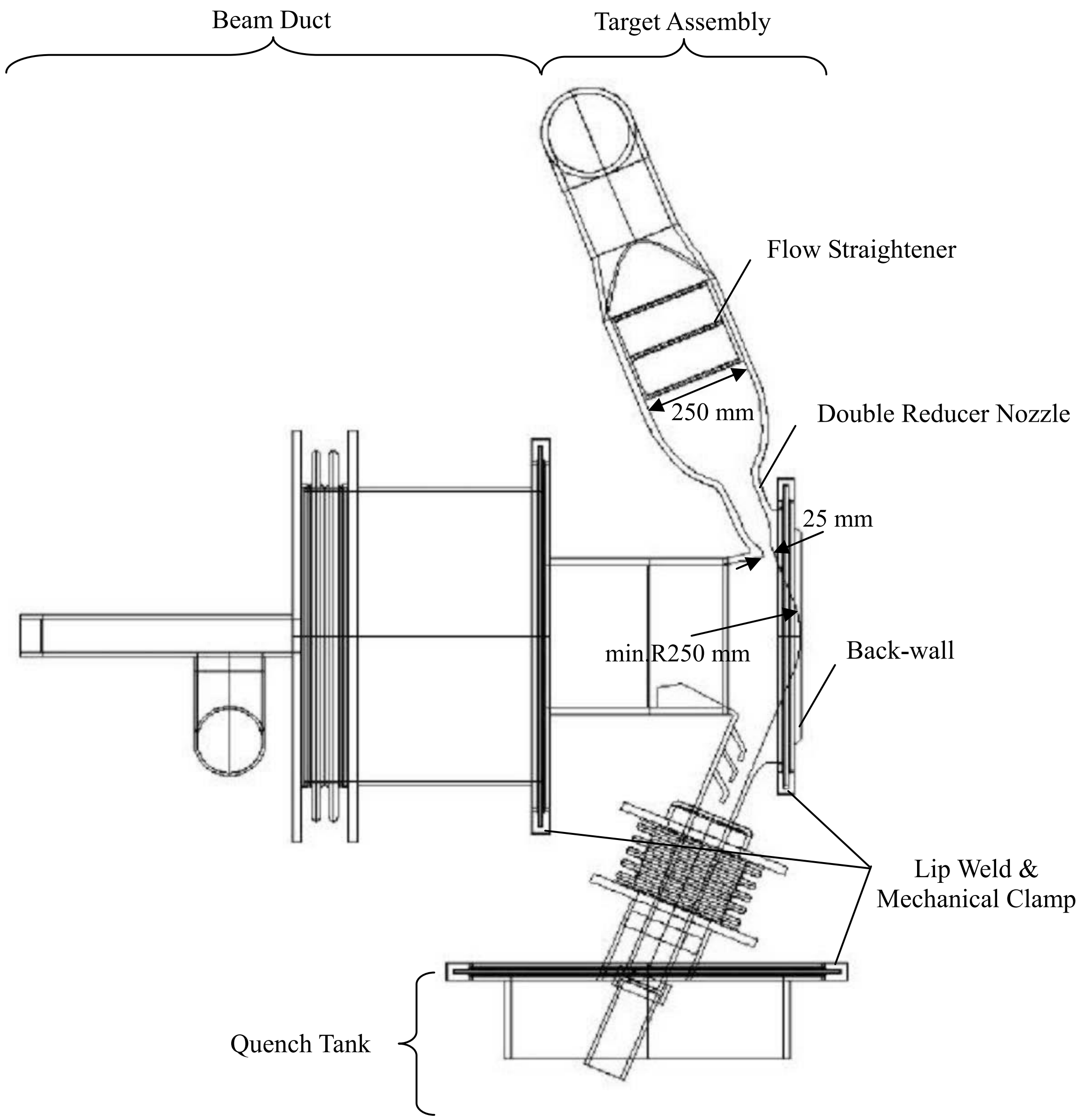

Fig. 2-3 Cross-section of IFMIF target assembly

3. Thermo-structural Analysis of the IFMIF Back-wall

3.1 Introduction

In the IFMIF [3-1], [3-2], intense neutrons are emitted inside the Li flowing on a thin back-wall attached to the target assembly. The target assembly is made of 316 L stainless steel alloy except for the back-wall which is made of Reduced-Activation Ferritic/Martensitic (RAFM) steel such as F82H and EUROFER. Since the back-wall is operating under severe neutron irradiation condition (50 dpa/y), the back-wall needs to be designed as a removable component which can be replaced by a remote handling system. Two design options for back wall replacement are under investigation. The first is called the “cut and reweld” option shown in Fig. 3-1. The back-wall is connected to the target assembly by a welded lip seal and a mechanical clamp at the circumference. For replacement of the back-wall itself, at first the overall target assembly is removed after disconnecting it by cutting the welded lip seals at the interface with fixed parts by using a remote Yttrium/Aluminum/Garnet (YAG) laser device. Secondly, the target assembly with the back-wall is transferred to the hot cell area and the back-wall is removed from the target assembly by another YAG laser cutting device [3-3]. The second option is called the “bayonet” option with mechanical attachment of the back-wall to the target assembly [3-4]. This option consists in replacing the back-wall from the target assembly without removing the target assembly itself from its position in the test cell. The back-wall removal is performed by a different remote handling device. Moreover, in the back-wall, the thermal stress is induced by the nuclear heating due to neutron irradiation. The maximum value of the nuclear heat generation was 25 W/cm^3 in the center region of the back-wall. Therefore, the thermo-structural design of the back-wall is one of the critical issues for the target design.

In this section, the latest efforts on the “cut and reweld” option aimed at optimizing the thermo-structural design of the lip seal back-wall concept are described.

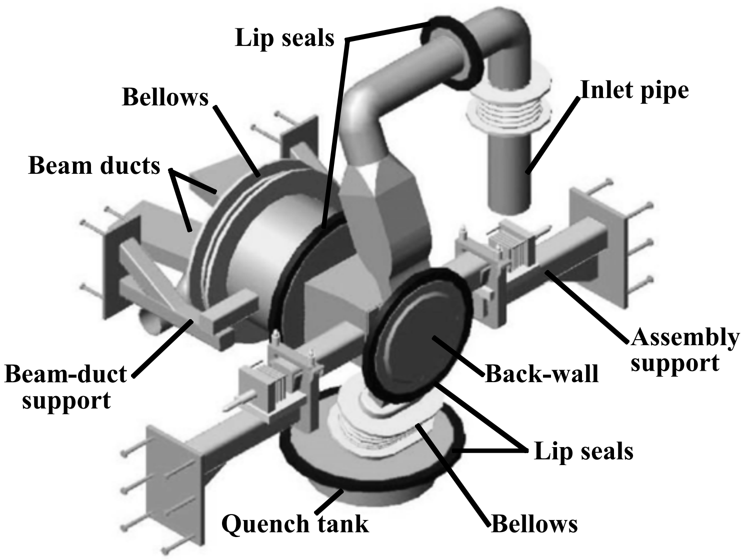

Fig. 3-1 Three-dimensional view of target assembly and back-wall

3.2 Calculation Model and Conditions

The thermal stress of the back-wall induced by the nuclear heating was estimated by using ABAQUS code with a linear analysis. In a previous thermo-structural analysis, a simple model independent of the target assembly shown in Fig. 3-2 was used [3-5]. Its shape is nearly a disc with a diameter of 0.715 m. Its Li flow side has a concave face with a radius of 0.25 m. The analysis was performed for 1/4 section (0 m < Y, 0 m < Z) of the back-wall because of its symmetry. Distribution of nuclear heating rate is also shown in Fig. 3-2. The maximum value of the nuclear heating rate was 25 W/cm^3 at beam center (Y = 0 m, Z = 0 m). Temperatures of the target assembly and liquid Li were both 300 °C, and thermal transfer coefficient between Li and the back-wall was 34 kW/m^2·K that was estimated as the minimum value from experimental results [3-6]. Emissivity of the back-wall was 0.3. Temperature of vertical test assembly (VTA) is assumed to be 50 °C because an effect of the VTA temperature from 50 °C to 150 °C on the back-wall temperature was found to be negligible. In the previous study [3-7], the allowable stress for the back-wall was assumed to be the yield strength because an inelastic deformation of the back-wall at its center region cannot be accepted. At the lip seal location, neutron irradiation is estimated to be from 0.1 to 1 dpa/y at full IFMIF performance while neutron irradiation at the back-wall central region is about 50 dpa/y. Therefore, in this study, the allowable stress for the lip seal is defined as the 3Sm value. According to ASME code, Sm is defined as the minimum value between (2/3)Sy and (1/3)Su where Sy is the yield strength and Su is the ultimate tensile strength. Figure 3-3 shows temperature dependences of the yield strength, tensile strength and 3Sm value for F82H [3-8] and 316L [3-9] steels in un-irradiated conditions. The allowable stresses defined by 3Sm for the 316L and the F82H at 300 °C are 330 MPa (=Sy) and 520 MPa (=Su), respectively. Since irradiated material data under condition similar to IFMIF are not yet available, the use of the un-irradiated material data has a safe margin considering radiation hardening although radiation embrittlement must be taken into account. The results showed that the von Mises stress of the F82H back-wall was about 300 MPa at its center. Although this value is below the allowable value defined by the yield strength, a more realistic model has to include the target assembly. Since an analysis which includes the real configuration of the target assembly is rather complex, an improved model was applied to include the effect of the target assembly on the thermo-structural behavior of the back-wall. In this model, a plate made of 316L stainless steel with a thickness of 30 mm was added behind the F82H back-wall as shown in Figs. 3-4(a) and 3-4(b). Around the 316L plate, there is a lip seal welded to the back-wall lip seal. However, this lip seal configuration was not acceptable due to high thermal stress (900 MPa). Therefore, to reduce the stress level, a stress mitigation structure consisting in a semi-circular annular bulge close to the lip seal is provided, as shown in Fig. 3-5. The inner diameter of the semi-circular bulge is 10 mm and the thickness of the lip seal is 5 mm. The boundary conditions are that the lip seals made of 316L stainless steel and F82H are welded at the edge. Around the leading edge region of the lip seal, mechanical clamps are also provided in order to fix together the welded lip seals, but the lip seals can still move in the radial direction.

In this analysis, creep and irradiation swelling were not considered in the deformation calculation, but the influences of these phenomena need to be evaluated in a future study.

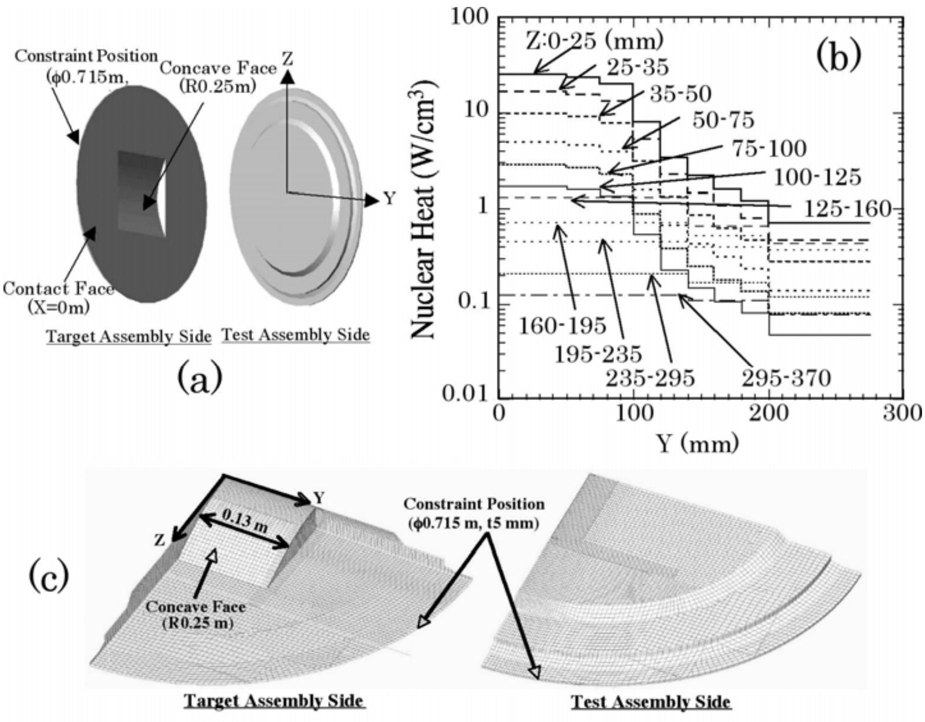

Fig. 3-2 Back-wall models and calculation conditions for the thermal stress analysis
(a) Back-wall model, (b) Nuclear heating rate and (c) ABAQUS model

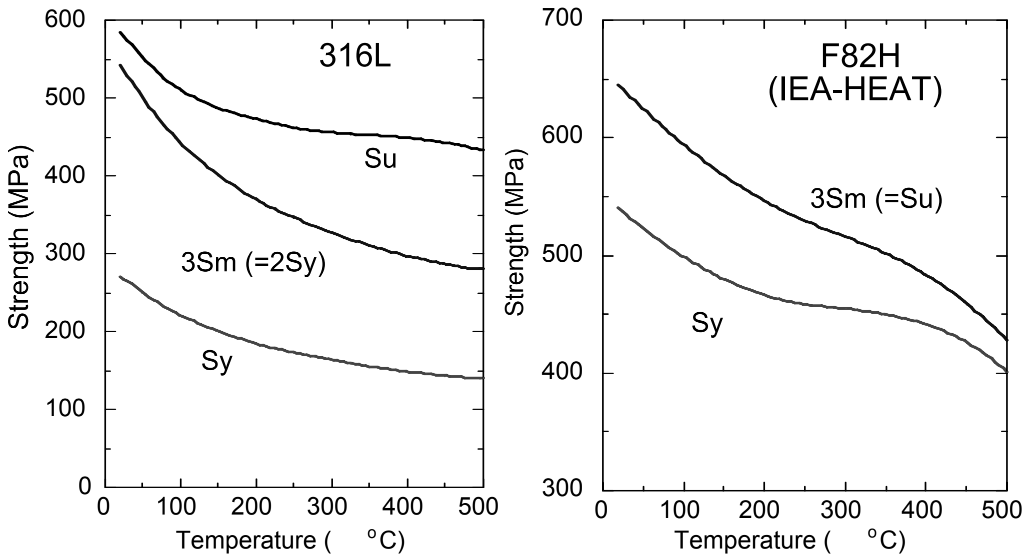

Fig. 3-3 Temperature dependences of mechanical strength of stainless steel 316L and F82H

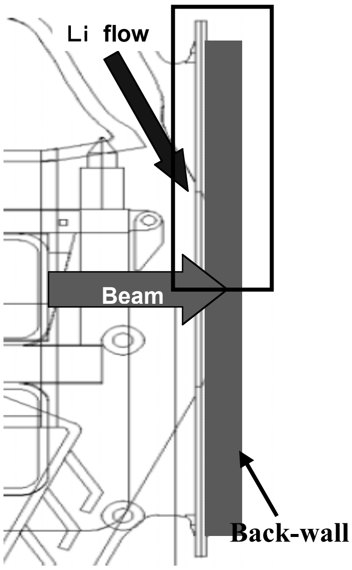

(a) Analysis region

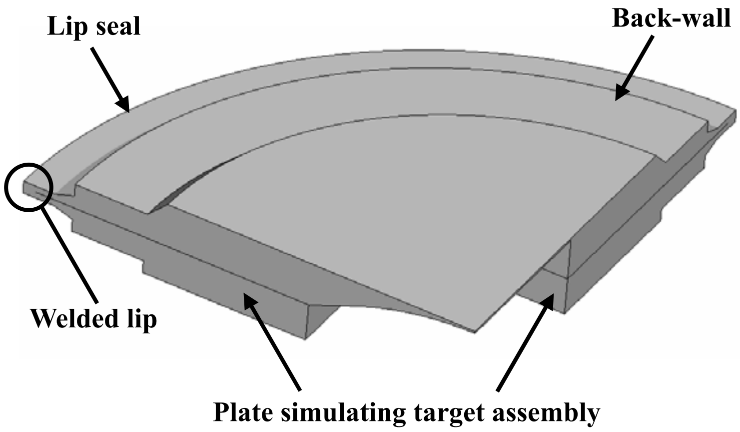

(b) Calculation model

Fig. 3-4 Back-wall model with a simplified target assembly

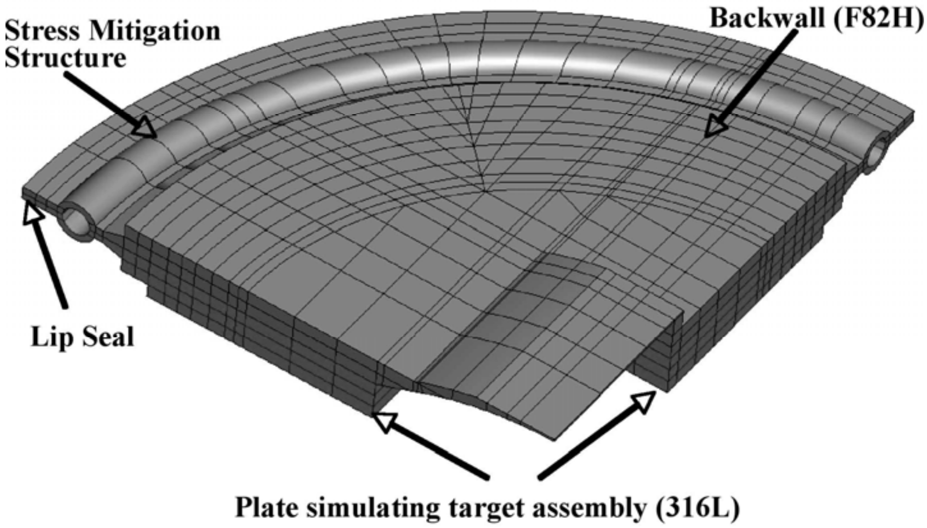

Fig. 3-5 Model of the back-wall with a stress mitigation structure

3.3 Results and Discussions

The results of the analysis of the lip seal with and without the stress mitigation structure in terms of deformation at back-wall center and von Mises stresses are summarized in Table 3-1. For comparison, the result of the previous analysis carried out on the base design [3-7] is also shown. In case of the lip seal design without stress mitigation structure, the von Mises stress at the lip seal was 910 MPa, thus beyond the permissible stress defined by the 3Sm, although the von Mises stress and the deformation at the back-wall center were reduced significantly. In case of the lip seal with stress mitigation structure, the contours of the temperature and the von Mises stress of the back-wall are shown in Figs. 3-6(a) and 3-6(b), respectively. The temperature of the back-wall at center is 300 °C i.e. the same as Li temperature. The maximum temperature (365 °C) occurs around the back-wall center. The maximum von Mises stress is 335 MPa occurring in the semi-circular stress mitigation structure of the lip seal. In this case, the von Mises stress and the displacement at the center of the back-wall are 93 MPa and 0.3 mm, respectively. Although the von Mises stress of the F82H lip seal is below the allowable stress, the von Mises stress of the 316L lip seal is slightly higher than the allowable stress. However, there are margins for an optimization of the 316L lip seal configuration, such as thickness and geometry, which could reduce the stress field and satisfy the allowable stress.

One of the main technical issues of the back-wall is the welding of the lip seal, which involves F82H and 316L stainless steels. Considering the existing welding technique for these materials, Tungsten Inert Gas (TIG) weld would be recommended. However, the TIG weld is not suitable for remote welding technique. On the other hand, in case of the weld of the 316L stainless steel to each other, Yttrium/Aluminum/Garnet (YAG) laser weld is suitable and applicable to the remote welding. Therefore, the lip seal improved concept was further modified and a specific assembly sequence was established. Prior to back-wall installation into the target assembly, the stress mitigation structure made of the stainless steel 316L is joined by TIG welding to the back-wall made of the F82H. Then, the back-wall is attached to the target assembly made of 316L by YAG laser welding by using a remote handling arm. The thermal stresses at the lip seal of the new concept are assumed to be similar to the improved model ones, as described in section 3.2, although a specific analysis will be necessary.

To evaluate material properties of these weldments, R&D of the lip seal weld is under way. After fabrication of welded specimens, examinations such as microstructure analysis, hardness and tensile tests shall be carried out to evaluate the performances of the weldment. The validation of the replaceable back-wall based on the “cut and reweld” concept by using a remote handling tool shall be performed during IFMIF EVEDA phase.

Table 1 The von Mises stress and deformation in the previous and improved models

	Previous Model	Improved Model
von Mises stress at BW center	107 MPa	93 MPa
at Lip seal	910 MPa	335 MPa
Deformation at BW center	0.25 mm	0.34 mm

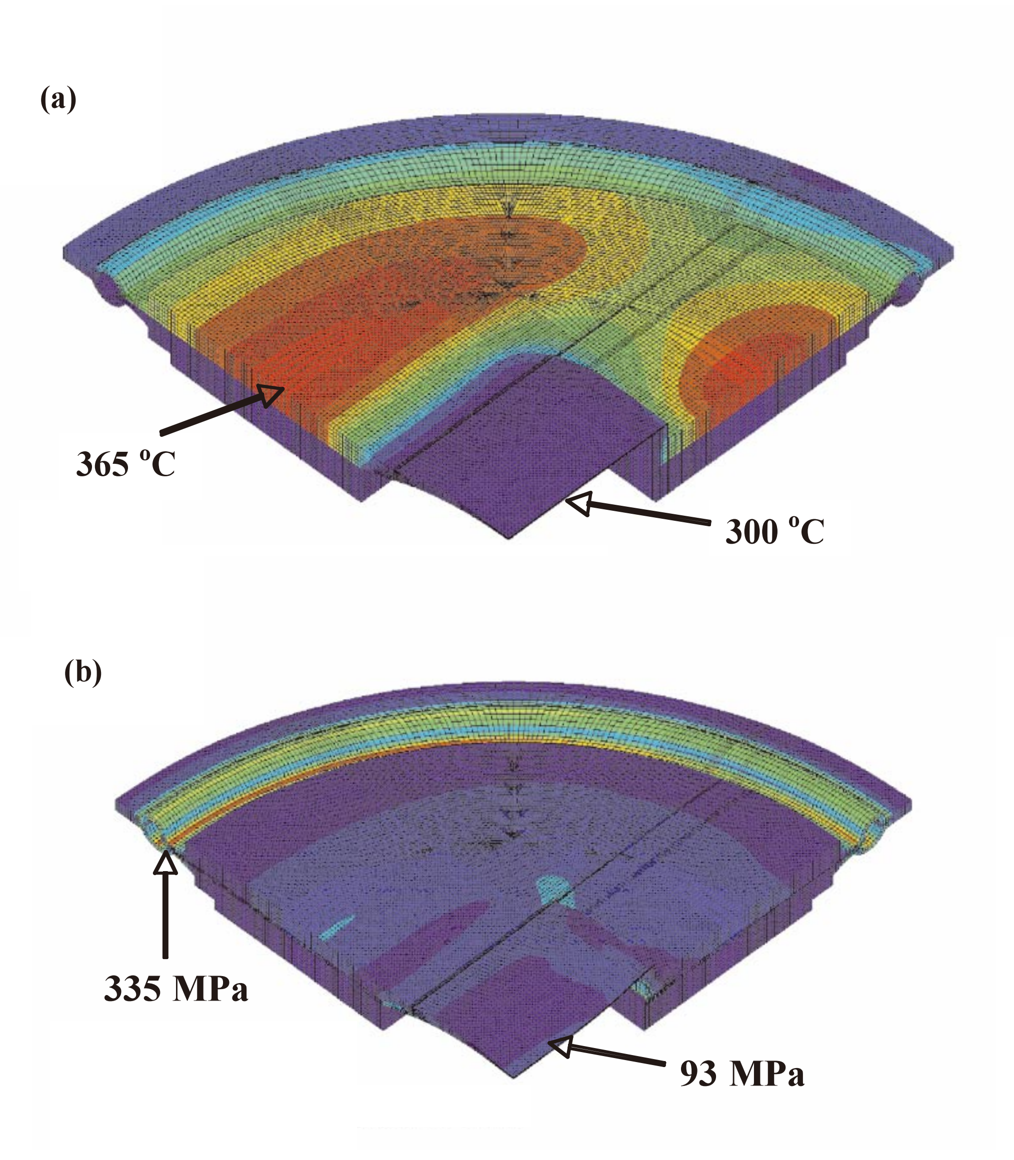

Fig. 3-6 Contours of temperature (a) and the von Mises stress (b) of the back-wall with a stress mitigation structure

3.4 Summary

Thermo-structural analysis of the “cut and reweld” type replaceable back-wall has been carried out by using the ABAQUS code. The improved model was applied to include an effect of the target assembly on the thermo-structural behavior of the back-wall. Moreover, to reduce thermal stress further, a lip seal with the stress mitigation structure was proposed. The maximum von Mises stresses of the back-wall (RAFM) and the lip seal (316L) were 93 MPa and 335 MPa, respectively. Although the von Mises stress of the 316L lip seal is slightly higher than the allowable stress defined by 3Sm, an optimization of the 316L lip seal configuration satisfies the allowable stress criterion. Considering the available welding techniques, a further modification of the improved model using the TIG and YAG weld is proposed. R&D on the lip seal weld is under way.

References

[3-1] A. Möslang, U. Fischer, V. Heinzel, P. Vladimirov, R. Ferdinand H. Klein, B. Riccardi, M. Gasparotto, H. Matsui, M. Ida, H. Nakamura, M. Seki, M. Sugimoto, H. Takeuchi, T. Yutani, T. Muroga, R. A. Jameson, T. Myers, J. Rathke, T. E. Shannon, S. Païdassi, V. Chernov, Proc. 19th Fusion Energy Conference, France, October 2002, IAEA-CN-94/FT1-2.

[3-2] IFMIF international team (Ed.) H. Nakamura, M. Ida, M. Sugimoto, M. Takeda, T. Yutani, H. Takeuchi, JAERI-Report, JAERI-Tech 2003-005, March 2003.

[3-3] H. Nakamura, B. Riccardi, K. Ara, L. Burgazzi, S, Cevolani, G. Dell’Orco, C. Fazio, D. Giusti, H. Horiike, M. Ida, H. Ise, H. Kakui, N. Loginov, H. Matsui, T. Muroga, Hideo Nakamura, K. Shimizu, H. Takeuchi, S. Tanaka, Fusion Eng. and Des. 66-68 (2003) pp.193-198.

[3-4] B. Riccardi, M. Martone, C. Antonucci, L. Burgazzi, S. Cevolani, D. Giusti, G. Dell’Orco, C. Fazio, G. Micciche, M. Simoncini, Fusion Eng. and Des. 66-68 (2003) pp.187-191.

[3-5] M. Ida, H. Nakamura, K. Shimizu, T. Yamamura, Fusion Eng. and Des. 75-79 (2005) pp.847-851.

[3-6] N. Uda, A. Miyazawa, S. Inoue, N. Yamaoka, H. Horiike, K. Miyazaki, J. Nucl. Sci. and Technol, 38 (2001) pp.936-943.

[3-7] H. Nakamura, M. Ida, T. Chida, K. Shiba, K. Shimizu, M. Sugimoto, J.Nucl.Mater. 367-370 (2007) pp.1543-1548.

[3-8] A.-A. F. Tavassoli, J.-W. Rensman, M. Schirra, K. Shiba, Fusion Eng. and Des. 61-62 (2002) pp.617-627.

[3-9] ITER Materilal Hand Book (ed. V. Barabash).

4. Preparation of Mechanical Tests for Welding Parts of Back-wall

4.1 Introduction

As mentioned in the Chapter 3, the back-wall made of the austenitic stainless steel 316L at its circumference part including the lip and the reduced-activation ferritic (RAF) steel F82H at its center part is preferable for integrity under the neutron irradiation condition in viewpoint of thermal-stress. For this reason, the back-wall and the target assembly have two types of welding part. One is remote cut/weld using YAG laser at an activated lip part made of 316L between the back-wall and a target assembly. Several sets of cut/weld will be done at one lip part during IFMIF operation in 30 years. The other is dissimilar welding between 316L and F82H within each back-wall. This welding is done only once for each back-wall in a factory before activation, thus will be done manually as tungsten inert gas (TIG) welding.

In general, mechanical properties of metal at weld zone consisting of weld metal and heat-affected zone (HAZ) are different from those at base metal (BM). For design of the back-wall and the target assembly, mechanical properties of not only BM of 316L and F82H but also the weld zone should be investigated. Also effects of weld conditions upon mechanical properties should be clarified. In FY2006, two types of weld specimens were fabricated and tested preliminarily as follows:

4.2 Fabrication of Weld Specimens

4.2.1 Type of specimen

For tensile tests and Vickers hardness tests on welded metals, specimens were fabricated. Eight types of specimen made of either/both of 316L and F82H steels as shown in Table 4.1 were fabricated. Two specimens were fabricated for each type. The total number of specimen is sixteen (2 x 8 = 16). Reference specimens T1, H1, T2 and H2 were made without welding. Specimens T3, H3, T4 and H4 were firstly welded and then mechanically cut. Size of each specimen is shown in Fig. 4.1. Corresponding to thickness of welded part in the IFMIF target back-wall/assembly, thickness of the welded specimen is 5 mm for 316L-316L specimens (welded by YAG laser) and 15 mm for 316L-F82H specimens (welded by TIG).

Table 4.1 ID number of specimen

Material / Purpose	316L	F82H	316L-316L	316L-F82H
Tensile test	T1-1 T1-2	T2-1 T2-2	T3-1 T3-2	T4-1 T4-2
Hardness test	H1-1 H1-2	H2-1 H2-2	H3-1 H3-2	H4-1 H4-2

4.2.2 Fabrication procedure

Corresponding to specimen materials, fabrication procedure including subsequent examination was carried out as shown in Table 4.2. Welded specimens are shown in Fig. 4.2.

Table 4.2 Fabrication procedure

Procedure \ Specimen ID (material)	T1-1, T1-2 H1-1, H1-2 (316L)	T2-1, T2-2 H2-1, H2-2 (F82H)	T3-1, T3-2 H3-1, H3-2 (316L-316L)	T4-1, T4-2 H4-1, H4-2 (316L-F82H)
Welding process	-	-	YAG	TIG (*1)
Post weld heat treatment	-	-	-	*2
Liquid penetrant testing	-	-	X	X
Radiographic test	-	-	X	X
Mechanical cutting	X	X	X	X
Polish	X	X	X	X
Measurement	X	X	X	X

*1 Filler metal: Y309, Wire speed: 30-90 cm/min, Torch speed: 6-10 cm/min, 100-180 A, 8.5-11 V

*2 Pre-heating: 150-200 °C, Heat treatment: 740 °C during 1 hr

4.3 Mechanical Tests

4.3.1 Microstructure of weld zone

Through microstructure observation (see Fig. 4.3) on cross-section of weld zone treated by using acids, it was found that most of the welding seemed to be done successfully, excepting that only one porosity with diameter of 0.5 mm in weld metal in a specimen H3 (YAG welding on 316L-316L). Small ferritic regions were observed near a center of double U groove in a specimen H4 (TIG welding on 316L-F82H).

4.3.2 Hardness tests on welded specimen

Vickers hardness tests were performed at room-temperature with indentations up to 9.8 N (test force) in 10 s (loading time), and interval more than 3d (3 times larger than dimple size) in a 30 mm-long region. The results are shown in Fig. 4.4. For specimens H3, the hardness was almost uniform in any part of the BM, HAZ and weld metal. For specimens H4, increase (max. 250HV) and decrease (min. 160HV) in the hardness occurred in the HAZ. Near the point of minimum hardness, a small ferrite-like region was observed as mentioned above.

4.3.3 Tensile tests

Tensile tests were performed at room-temperature with stress rate 0.1 and 30 mm/min respectively below and beyond the yield stress for the specimens T3, and 0.5 and 30 mm/min for the specimens T4, in accordance with Japanese Industrial Standard. Note that cross section of the specimens were reduced to ^{T}5mm x ^{W}6 mm for T3 and ^{T}15mm x ^{W}6 mm for T4 after re-fabrications, to fracture well within a capacity of the test machine. The results are shown in Fig. 4.5 and Table 4.3. For specimens T3, ultimate tensile stress (UTS) was 464 MPa less than the value 553 MPa for non-weld specimens T1. Fractures occurred in each weld zone where Vickers hardness was 165 MPa the minimum as shown in Fig. 4.3. On the contrary, for specimens T3, UTS was 575 MPa roughly equal to the value 553 MPa for T1. Fractures occurred in each BM of 316L. Integrity of weld zone was confirmed for the dissimilar welding between 316L and F82H using the filler metal Y309.

Table 4.3 Results of tensile tests (averaged values)

	T1	T2	T3	T4
UTS (MPa)	553	631	464	575
Elongation (%)	47	19	34	24

4.4 Summary

Preliminary fabrication and tests of the welding specimens were done. Most of the welding seemed to be done successfully for both of YAG welding on 316L-316L and TIG welding on 316L-F82H. For the specimens of 316L-316L welding, the hardness was almost uniform in any part. For the specimens of 316L-F82H welding, increase and decrease in Vickers hardness occurred in the HAZ. UTS of the specimens of 316L-316L welding was less than that of non-weld specimens, and fractures occurred in their weld zone. On the contrary, UTS of the 316L-F82H welding was roughly equal to that of non-welding specimens, and fractures occurred in BM of 316L. This showed integrity of the 316L-F82H welding using the filler metal Y309.

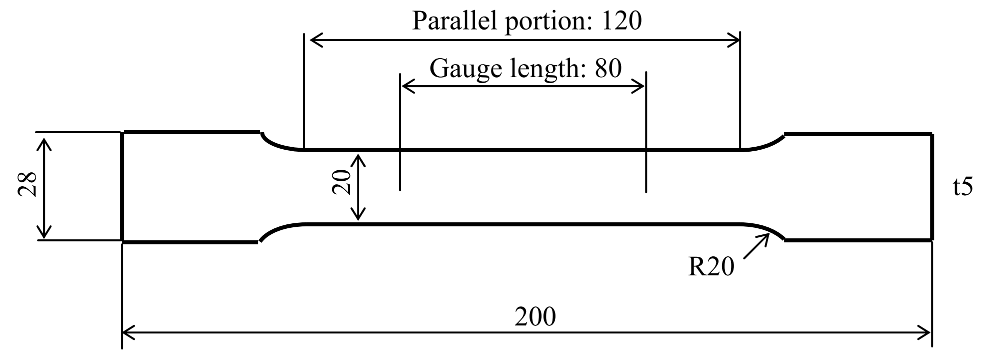

Specimen for tensile tests (without welding, ID: T1, T2)

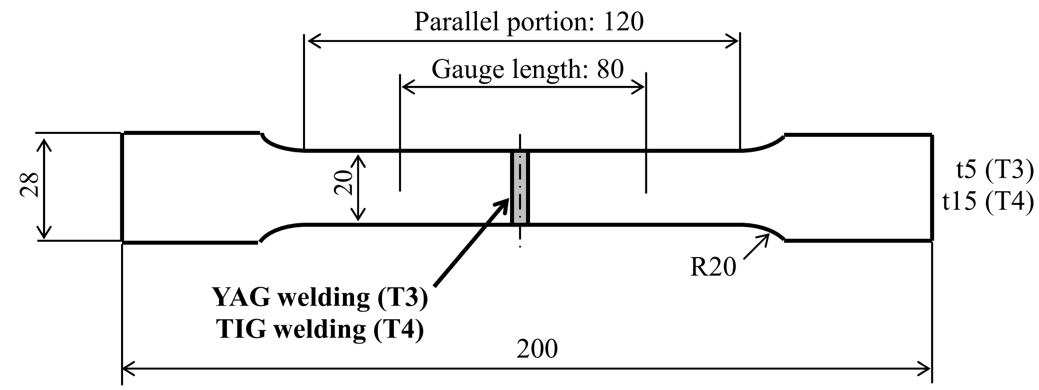

Specimen for tensile tests (with welding, ID: T3, T4)

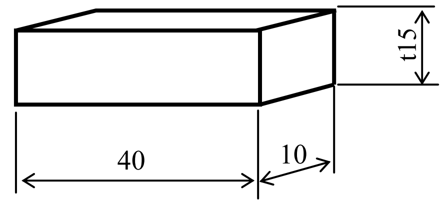

Specimen for hardness tests
(without welding, ID: H1, H2)

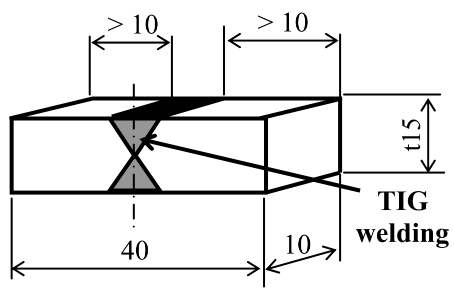

Specimen for hardness tests
(with welding, H4)

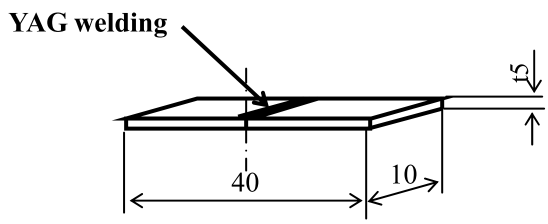

Specimen for hardness tests
(with welding, ID: H3)

Fig. 4.1 Specimen size

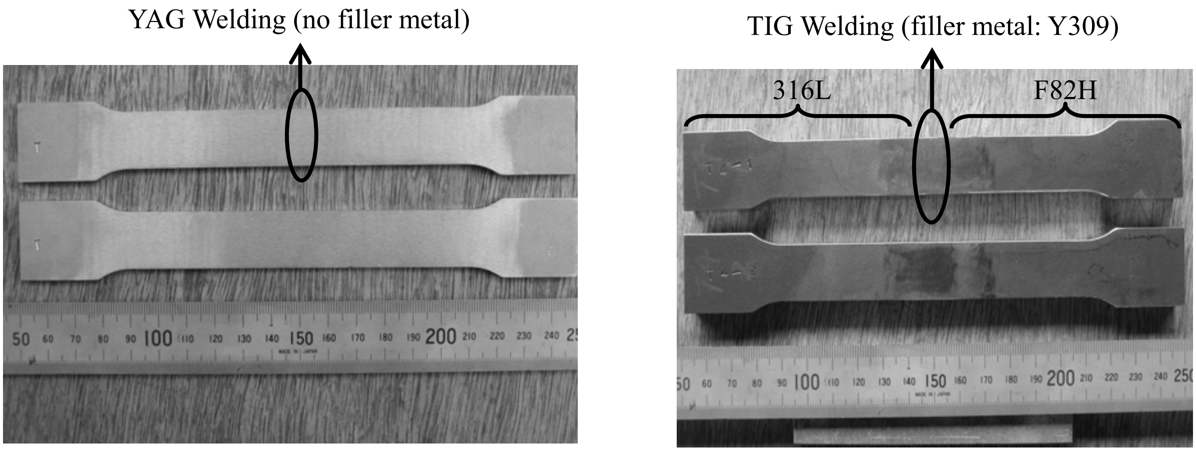

316L-316L (t5mm, ID: T3)

316L-F82H (t15mm, ID: T4)

Fig. 4.2 Welded specimen for tensile test

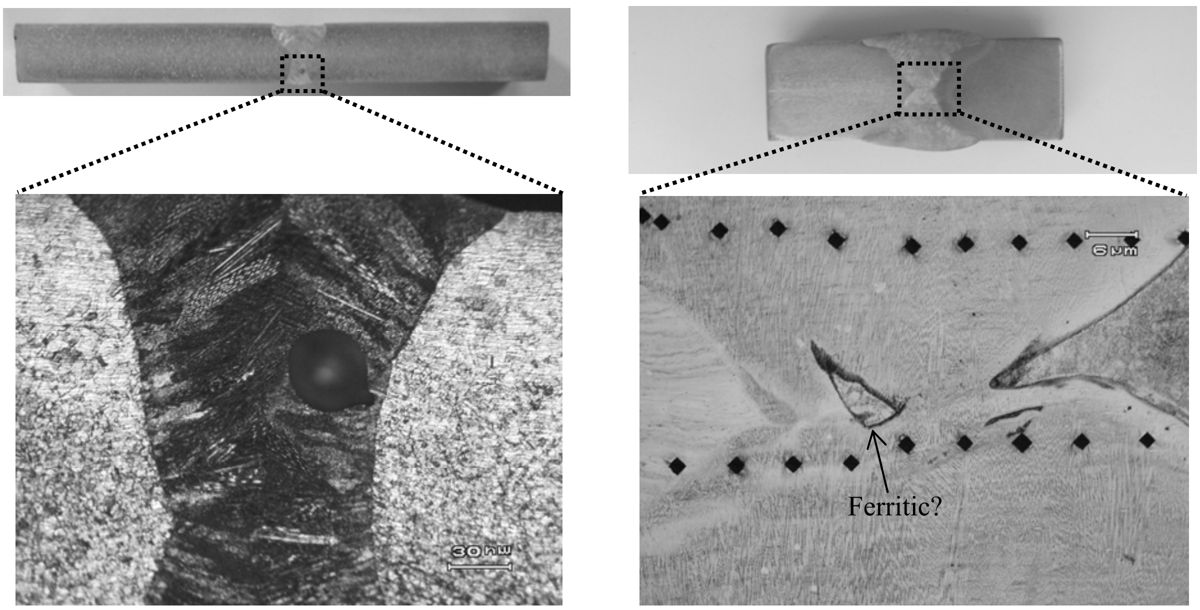

316L-316L (ID: H3)

316L-F82H (ID: H4)

Fig. 4.3 Welded specimen for hardness test

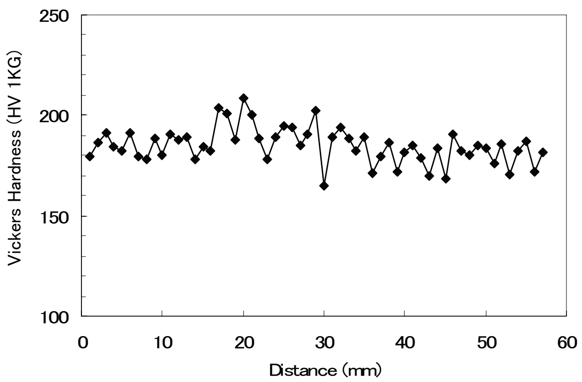

316L-316L (ID: H3)

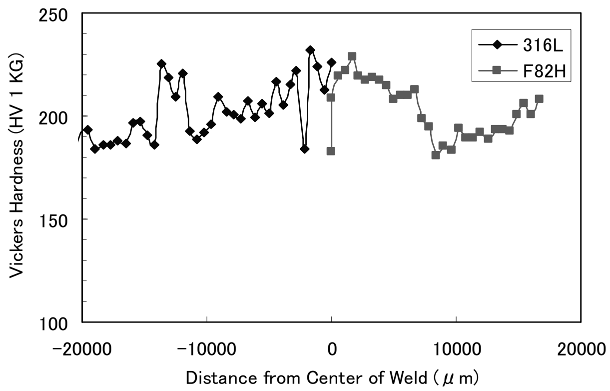

316L-F82H (ID: H4)

Fig. 4.4 Vickers hardness of welded specimen

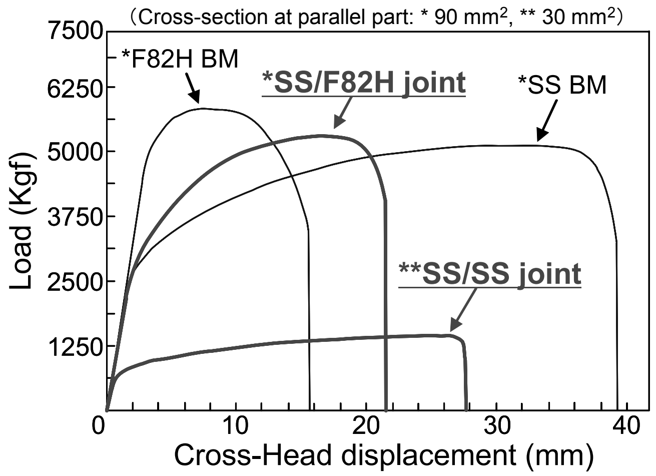

Fig. 4.5 Stress-strain curves

5. Estimations on Behavior of Beryllium-7 and Control of Worker Dose

5.1 Introduction

In the IFMIF target, many types of radioactive nuclide are produced as shown in Figs. 5.1 and 5.2. They are tritium (T or ^{3}H) and beryllium-7 (^{7}Be) through deuteron-lithium (D-Li) reactions, and metallic nuclides corroded from inner walls of Li components activated by neutrons. These radioactive nuclides affect worker dose at annual maintenance of the components carried out within one month after every eleven months operation of IFMIF. A guideline of dose equivalent rate is 10 μSv/h derived from an ICRP-60 recommendation 100 mSv in five years and maximum yearly working time of 2,000 h.

The back-wall is most activated by neutrons among the IFMIF components. Its activation and consequent worker dose were estimated with assuming a corrosion rate 1 μm/year from the back-wall surface and uniform deposition of metallic radioactive nuclides on all components surface wetted by Li. The result was acceptable. [5.1] Also behavior of T generated and accumulated in the IFMIF target system was estimated. The result showed that T release rate from the components wall would be 1.0×10^{6} Bq/h. [5.2] This value is enough lower than the designed capacity of tritium treatment system of IFMIF.

With the background above mentioned, recent study for worker dose has been focused on effects of ^{7}Be. Radioactivity of ^{7}Be is 5.02×10^{15} Bq, and each nuclide of ^{7}Be emits a gamma ray with energy of 0.478 MeV. In the previous study, effects of ^{7}Be were estimated by a calculation code with a simplified assumption that the all ^{7}Be uniformly deposit on the components wall wetted by Li. The result showed that 89% of the deposit on inner wall of the heat exchanger (HX) due to the large surface area of 576 m^2, and thus a 22cm-thick iron (Fe) shield or a 6.5cm-thick lead (Pb) shield is required to reduce the worker dose around the HX to the limit 10 μSv/h. [5.3] However, more precise estimation is needed for design of the Li components and their radiation shielding, and planning maintenance scenario. Therefore, behavior of ^{7}Be such as solubility and deposition in liquid Li depending temperature, and radiation shielding / shutdown scenario of the Li loop to control worker dose below the limit, were estimated and investigated.

5.2 Estimation of ^{7}Be Behavior in IFMIF Li Loop

Estimation of 7Be in the Li loop was performed, with focusing on temperature-dependent solubility. A deposition location of 7Be in the Li loop with temperature gradient was identified, by using solubility data obtained previous experiments.

5.2.1 Radio activity of ^{7}Be in IFMIF Li loop

Beryllium-7 is generated through the reactions $^{6}Li(D, n)^{7}Be$ and $^{7}Li(D, 2n)^{7}Be$ in the target area. The generation rate of is estimated to be 5.02×10^{15} Be/s, using the production ratio of $^{7}Be/D$ of 0.00322 with accuracy of ±12% in the case of incident deuteron energy of 40 MeV [5.4, 5.5] and the beam current of 250 mA. The radioactivity of ^{7}Be soon reaches an equilibrium condition at 5.02×10^{15} Bq, since the half-life is only 53.3 days. In the Li loop with Li inventory of 4.5×10^{3} kg, the ^{7}Be exist in bound (Be_3N_2) and unbound (pure ^{7}Be) forms. An atom ratio of ^{7}Be (in any forms such as bound / unbound, solved / deposited) to Li: C_{Be} is 8.63×10^{-8} under the equilibrium condition. An increase in ^7Be concentration at the target area: ΔC_{Be} is 8.73×10^{-13} as the atom ratio in a typical case of flow rate 0.13 m^3/s.

5.2.2 Solubility of ^7Be in IFMIF liquid Li

In the Fusion Materials Irradiation Test facility (FMIT) project preceding IFMIF, a solubility of ^7Be in liquid Li was measured and estimated as a condition of chemical equilibrium with nitrogen (N). This condition was found to be as follows:[5.6]

$$\log_{10}(C_N^2 C_{SBe}^3) = -5.7 - 20{,}300/T \qquad (5.1)$$

where T is temperature in K, and C_N and C_{SBe} are atom ratios of respectively N and unbound Be to Li under equilibrium with Be_3N_2. The compound Be_3N_2 would be deposited due to its density 2.73×10^3 kg/m^3, several times higher than the Li density 5.10×10^2 kg/m^3 at 250 °C. In the IFMIF design, C_N is to be controlled at 4.95 appm (10 wppm) by a hot trap in Li purification system. The value C_N is assumed to be constant, since C_N is far lager than C_{Be} and C_{SBe} ($C_N >> C_{Be}$ and $C_N >> C_{SBe}$). Based on the equation (5.1), and as shown in Fig. 5.3, C_{SBe} is 5.04×10^{-12} at 250 °C and 3.26×10^{-11} at 285 °C. These values are much lower than mentioned ^7Be concentration: C_{Be} 8.63×10^{-8} ($C_{SBe} << C_{Be}$). Therefore, in the IFMIF case, most ^7Be would be deposited in the Li loop in the form of Be_3N_2.

5.2.3 Deposition of ^7Be in IFMIF Li loop during operation

At any temperature, the concentration of unbound ^7Be: C_{UBe} is to be equal to the solubility: C_{SBe} or less ($C_{UBe} \leq C_{SBe}$). A simplified scenario of ^7Be behavior including the increase at the target area and deposition at low-temperature regions was considered to be continuously repeated as follows.

1) At the upstream location of the target area, the flowing Li contains unbound ^7Be with the saturation in concentration as the atom ratio of 5.04×10^{-12} at 250.0 °C

$$C_{UBe} = C_{SBe}(250\ °C) = 5.04 \times 10^{-12} \text{ (atom ratio)} = 5.04 \times 10^{-6} \text{ appm}$$

2) Within the target area, the ^7Be concentration is increased from 5.04×10^{-12} to 5.91×10^{-12} by the D-Li reactions adding ΔC_{Be}: 8.73×10^{-13}. At the same time, the unbound ^7Be solubility is increased from 5.04×10^{-12} to 3.26×10^{-11} depending on temperature change from 250.0 °C to 285.0 °C.

$$C_{UBe} = C_{SBe}(250\ °C) + \Delta C_{Be} = 5.91 \times 10^{-12}$$

3) At the down stream location of the target area, all unbound ^7Be can be solved due to the solubility of 3.26×10^{-11} much higher than the concentration of 5.91×10^{-12}.

$$C_{UBe} < C_{SBe}(285\ °C)$$

4) After the beam heating, the Li flows at the flow rate Q: 0.13 m^3/s through the quench tank and pipes with diameter of 250 mm. A small part of Li flow is divided from the main flow and provided to a Li purification system consisting of a cold trap and two hot traps. In the cold trap, flow rate: Q_{CT} is 2.5×10^{-4} m^3/s and the minimum temperature is 200.0 °C, which corresponds to solubility of

2.16×10^{-13}. After re-joining of this small flow at 2.5×10^{-4} m^3/s with the concentration of 2.16×10^{-13} and remaining main flow of 0.12975 m^3/s with the concentration of 5.91×10^{-12}, the average concentration of main flow is slightly reduced to 5.90×10^{-12} at flow rate 0.13 m^3/s.

$$C_{UBe} = \{(Q-Q_{CT})/Q\}\{C_{SBe}(250\ °C) + \Delta C_{Be}\} + (Q_{CT}/Q)\{C_{SBe}(200\ °C)\} = 5.90 \times 10^{-12}$$

5) In a part of HX, the additional concentration of ^7Be, except for the small part provided to the cold trap, is deposited in the form of Be_3N_2. Temperature of the location of deposition onset is 252.8 °C corresponding to the concentration of 5.90×10^{-12}. Therefore, main region of the deposition is the most downstream part (approximately 1/10 part) of the HX.

$$C_{UBe} = C_{SBe}(250\ °C) = 5.04 \times 10^{-12}$$

then, the scenario goes to 1). The concentration of unbound ^7Be, temperature and flow rate of the liquid Li were schematically summarized in Fig. 5.4.

In this scenario, it was assumed that a reaction to composite Be_3N_2 and its deposition on inner walls of components immediately occur. In the HX, the Li flows at the lowest flow velocity due to the largest cross section of flow among the Li components in the main flow. Furthermore, the Li flow in the HX is the most complex due to the HX structure consisting of twelve (12) sets of baffle and four hundred and thirty-four (434) sets of U-tube for the organic oil as shown in Fig. 5.5. From a viewpoint of flow condition, the HX is the first candidate of Be_3N_2 deposition occurrence under saturated condition of ^7Be.

5.2.4 Identification of locations with high radioactivity after shutdown

Radioactivity in each Li component depends on shutdown procedure of the Li loop after the beam stop. In this estimation, the radioactivity of ^7Be in two cases of the shutdown was estimated as follows:

<u>Case-1: Immediate Li drain to the dump tank after the beam stop</u>

Even with the higher concentration of unbound ^7Be of 5.91×10^{-12}, radioactivity due to the unbound ^7Be in the Li inventory of 4.5×10^3 kg is only 3.44×10^{11} Bq, far smaller than the total radioactivity of 5.02×10^{15} Bq. Most of this relatively small radioactivity in the liquid Li can be drained into the dump tank before worker access for maintenance. In this estimation, a small fraction of liquid Li with thickness of 1 mm was assumed to remain on inner walls of pipes. However, more than 99.99% of the total radioactivity would remain in the form of Be_3N_2 on the inner wall around the most downstream part of HX (98.72%) and in the cold trap (1.27%). Table 5.1 shows radioactivity of ^7Be in typical components: the Heat Exchanger (HX) containing Be_3N_2, the Cold Trap (CT) containing Be_3N_2, the Dump Tank (DT) containing unbound ^7Be, and the longest Pipe of ^{L}6.5 m, ^{ID}199.9 mm containing unbound ^7Be in Case-1.

<u>Case-2: Li circulation with trapping by the cold trap</u>

In this case, even after the beam stop, the liquid Li is circulated through the main loop including HX and the purification loop including CT. Operation temperature of CT is 200 °C, and temperature of the other component is higher than 200 °C, then most of ^7Be deposited as Be_3N_2 in HX is re-solved and deposited in HX. Concentration of unbound ^7Be remaining in the liquid Li is 2.16 x 10^{-13}, equal to Be solubility at 200 °C. As shown in Table 5.1, more than 99.999% of the total radioactivity would remain in CT, and less than 0.001% in the other component. Table 5.1 shows radioactivity of ^7Be in HX containing unbound ^7Be in liquid Li with thickness of 1 mm remaining on its inner-wall with area of 576 m^2, in CT containing Be_3N_2, in DT containing unbound ^7Be, and in the longest Pipe containing unbound ^7Be, in Case-2.

Note: A duration required for the re-trapping scheme in Case-2 depends on design of IFMIF target system. In the present design, flow rate of cold trap (Q_{CT}) is 0.25 L/s, operation temperature of main loop is 250-285 °C, design temperature of Li component is 400 °C (quench tank) / 350 °C (others). Required time for the re-trapping is at least 522 days (300 °C), 58.8 days (350 °C) or 9.18 days (400 °C). If flow rate of CT is increased to 0.5 L/s and main loop is operated at temperature 350 °C, the re-trapping will be done in the annual maintenance time of 1-month. Also re-trappings in weekly maintenance with 8 h/week are effective to save the time.

Table 5.1 Radioactivity of ^7Be after Li drain (unit: Bq)

	HX	CT	DT	Pipe (^{L}6.5 m)
Case-1	4.96 x 10^{15}	6.30 x 10^{13}	3.44 x 10^{11}	1.55 x 10^8
Case-2	8.03 x 10^8	5.02 x 10^{15}	1.26 x 10^{10}	5.67 x 10^6

5.3 Estimation of Worker Dose around Li Components Containing ^7Be

With identification of Li components containing ^7Be as shown in Table 5.1, it was clarified that the heat exchanger (HX) and the cold trap (CT) were the dominant components for worker dose. Dose equivalent rate around the typical components shown in Table 5.1 with/without radiation shield was estimated using the calculation code QAD-CGGP2R, which was revised from QAD-CGGP2 [5.7] to provide a dose equivalent rate.

5.3.1 Calculation conditions

For simplified and conservative estimation, calculation conditions were assumed as follows. All the radioactivities of ^7Be shown in Table 5.1 were assumed to be deposited uniformly in every component. As shown in Table 5.2, the HX length as radioactive source in Case-1 was 0.79 m, since most of ^7Be is deposited in the 1/10 downstream part of HX in Case-1. HX was assumed to be a volumetric source even in Case-2, since ^7Be in Case-2 is in thin Li layer of 1 mm on surface of 434 sets of U-tube arranged almost uniformly in the HX vessel as shown in the cross-section A-A in Fig. 5.5. In the same sense, also CT was assumed to be a volumetric source. DT is a volumetric source, since it contains most of liquid Li after drain. Pipe was assumed to be an area source, since it contains only one thin layer of the liquid Li with thickness 1 mm on the inner surface. A nuclide ^7Be decays to ^7Li through an electron capture. The decaying ^7Be emits a gamma ray with energy of 0.478 MeV and a probability of 0.105. These values also were inputted.

In the case of no-shielding, only the outer walls of HX, CT, DT and Pipe as shown Table 5.2 were inputted. Only this wall functions as a radiation shield in case of no-shielding. Shielding effect due to the U-tubes in HX was ignored. This assumptions produce slightly conservative results. In the case of shielding, lead (Pb) was chosen as a shielding material. The thickness of the Pb-shield sufficient to control the worker dose less than the limit 10 μSv/h was determined by try and error of the calculation.

Table 5.2 Dimension of Li component model as radioactive source

<table>
<tr><th></th><th>HX</th><th>CT</th><th>DT</th><th>Pipe</th></tr>
<tr><td>Outer wall</td><td>$^{D}1.1$m + $^{T}15$ mm
$^{L}7.9$m + $^{T}15$mm</td><td>$^{D}0.75$m + $^{T}9$mm
$^{L}1$m + $^{T}40$mm</td><td>$^{D}1.66$m + $^{T}20$ mm
$^{L}5.96$m + $^{T}20$mm</td><td>$^{D}0.1999$m
+ $^{T}8.2$ mm</td></tr>
<tr><td>Source (Case-1)</td><td>$^{D}1.1$ m, $^{L}0.79$ m</td><td rowspan="2">$^{D}0.55$ m
$^{L}0.65$ m</td><td rowspan="2">$^{D}1.66$ m
$^{L}5.96$ m</td><td rowspan="2">$^{ID}0.1979$ m
$^{OD}0.1999$ m
$^{L}6.5$ m</td></tr>
<tr><td>Source (Case-2)</td><td>$^{D}1.1$ m, $^{L}7.9$ m</td></tr>
</table>

The calculation code employed is QAD-CGGP2R to deal with three-dimensional (3-D) problems of the radioactive source, buildup factors within the component wall (and a Pb-shield in the shielding cases), and estimation points (i.e. detector locations). The volumetric source in HX was divided into ninety-six (96) elements in the circumference direction: θ ($\Delta\theta = 3.75°$), ninety-eight (98) in the length: L (non-uniform mesh, minΔL = 0.5 mm, maxΔL = 25 mm in Cese-1, minΔL = 5 mm, maxΔL = 250 mm in Cese-2) and fifty-five (55) in the radial direction: R (ΔR = 10 mm). Dividing manner for each component is summarized in Table 5.3. Each small radioactive source ($\Delta\theta \bullet \Delta L \bullet \Delta R$) is assumed by the code to be a point source, the code then calculates dose equivalent rate as the sum of those due to the point sources. This discrete method caused estimation error, for example of HX, less than 1 % in dose equivalent rate at 1cm from the HX wall or farther (R ≥ 0.575 m).

Table 5.3 Dividing of radioactive source in each component

	HX	CT	DT	Pipe
Δθ	3.75° x 96	3.75° x 96	3.75° x 96	15° x 24
ΔR	10mm x 55	5mm x 55	10mm x 83	1mm x 1
ΔL	0.5-25mm x 98 (Case-1) 5-250mm x 98 (Case-2)	5-10mm x 90	10-80mm x 98	5-250mm x 98

The component walls were assumed to be made of 316L stainless steel with density of 7.98 x 10^3 kg/m^3 consisting of Fe (66 %), Cr (16%), Ni (12%), Mn (2%), Mo (2%) and Si (1%). The remaining fraction 1% for other rare elements was ignored in the calculation. In the cases of shielding, Pb shield with density of 7.98 x 10^3 kg/m^3 was set on each outer wall. The atomic number and the partial density influence the buildup factor and the shielding performance. For examples, attenuation coefficient to the 0.478 MeV gamma ray was 1.62 x 10^{-2} m^2/kg for Pb and 8.46 x 10^{-3} m^2/kg for Fe in this calculation.

Only Pb was selected as the shield material due to the high attenuation coefficient and high density, as mentioned above.

5.3.2 Results and discussion

Case-1: Immediate Li drain to the dump tank after the beam stop

Calculated dose equivalent rate: $\dot{H}$ (= dH/dt) around the HX, CT, DT and Pipe without shield in Case-1 is shown in Fig. 5.6. In the case of no-shield, $\dot{H}$ at a location 1 cm from the wall (R = 0.575 m for HX, 0.384 m for CT, 0.86 m for DT, 0.11815 m for Pipe, respectively) is respectively 8.4×10^7, 2.5×10^6, 5.5×10^2 and 3.2 μSv/h. Any radiation shield is need for pipes, considering the guideline 10 μSv/h for yearly work time of 2,000 h. Also DT will not need any radiation shield, if time of annual maintenance contacting DT is limited less than 36 h. Furthermore, DT is installed in a pit below a level of a Li Loop Area where other Li components are installed. On the contrary, $\dot{H}$ at HX without a shield is about seven orders of magnitude higher than the limit 10 μSv/h. If the dose: H is to be reduced by limiting the work time only, the permitted yearly work time is only about 2×10^{-4} h, not realistic. As shown with a broken line in Fig. 5.7, the $\dot{H}$ is inverse proportional to square of the distance from HX center: R ($H \propto R^{-1}$) in a region 1m from the HX center or farther (R ≥ 1 m). In this spatial region, the radioactive source in the 1/10 part of HX seems to be a point source. If the dose: H is to be reduced by access control with distance, a needed R is more than 1,600 m, not realistic. Furthermore, if a cooling time is one month in annual maintenance, $\dot{H}$ is reduced by 1/1.5 only, since the half-life of ^{7}Be is 53.3 days. Also $\dot{H}$ at CT without a shield is about six orders of magnitude higher than the limit 10 μSv/h. This requires limit on annual working time less than 8×10^{-3} h or access control more than 200 m (see Fig. 5.8), both are not realistic.

Other measures are needed to carry out the yearly (if needed) maintenance of the Li components. Effects of radiation shielding were estimated. Calculated dose equivalent rate: $\dot{H}$ in the case of shielding also is shown in Figs. 5.7 and 5.8. To reduce the $\dot{H}$ below 10 μSv/h, needed thick ness of Pb-shield was found to be 8 cm for HX and 7 cm for CT. Weight of the Pb-shield around CT is 3.3 tons. On the contrary, weight of the Pb-shield around 7.9 m-long HX is 30 tons, far larger than the weight of the HX 10.4 tons. Shield thickness can be reduced by combination with a time control at maintenance. For an example, in case of yearly maintenance near HX and CT is limited less than 200 h (i.e. only the scheduled maintenance in one month), the sufficient thickness of shield is respectively 7cm and 6 cm. However, no significant reduction in Pb weight can be expected in Case-1.

Case-2: Li circulation with trapping by the cold trap

Calculated dose equivalent rate: $\dot{H}$ (= dH/dt) around the HX, CT, DT and Pipe without shield in Case-2 is shown in Fig. 5.9. In the case of no-shield, $\dot{H}$ at a location 1 cm from the wall is respectively 2.0, 2.0×10^8, 20 and 0.12 μSv/h. $\dot{H}$ at HX, DT and Pipe was significantly reduced from each value in Case-1, since most of ^{7}Be is re-trapped in CT. The Li components excepting CT do not need radiation shields. On the contrary, $\dot{H}$ at CT was significantly increased. However, increase in thickness of needed Pb-shield was only 2 cm (see Fig. 5.10) and weight of the Pb-shield was 4.4 tons. This shutdown scheme (Case-2) is a candidate of measure to control the worker dose.

5.4 Summary

Solubility of beryllium (Be) in liquid lithium (Li) is very low even under well-controlled nitrogen (N) level of 10 wppm. Most of ^{7}Be generated through deuteron-lithium (D-Li) reactions with rate of 5.02 x 10^{15} Be/s is deposited in the form of Be_3N_2 in rather cold location, such as the heat exchanger (HX) and the cold trap (CT), among the IFMIF LI loop.

In case of immediate Li-drain to the dump tank (DT) after D beam stop (Case-1), more than 99.99% of the total radioactivity 5.02 x 10^{15} Bq would remain in the form of Be_3N_2 on the inner wall around the most downstream part of HX (98.72%) and in the cold trap (1.27%). In case of Li circulation with trapping by CT (Case-2), more than 99.999% of the total radioactivity would remain in CT, and less than 0.001% in the other component.

In Case-1, dose equivalent rate around HX and CT without radiation shields was respectively 8.4 x 10^7 and 2.5 x 10^6 μSv/h, several orders higher than a guideline of 10 μSv/h. Both of limitation in working time and control on access distance are not effective to control worker dose at maintenance of HX and CT. Thickness of needed radiation shield made of lead (Pb) is 8 cm for HX and 7 cm for CT, and weight of Pb-shield is 30 tons for 7.9 m-long HX and 3.3 tons for CT. Employment of the shutdown scheme Case-2 significantly reduce the total weight of Pb-shield from 33 tons to 4.4 tons, since Pb-shield around only CT (thickness: 9 cm, weight: 4.4 tons) is needed in this case.

References

[5.1] H. Nakamura, M. Takemura, M. Yamauchi, U. Fischer, M. Ida, S. Mori, T. Nishitani, S. Simakov and M. Sugimoto, Accessibility Evaluation of the IFMIF Liquid Lithium Loop Considering Activated Erosion/Corrosion Materials Deposition, Fusion Engineering and Design 75-79 (2005) pp.1169-1172.

[5.2] K. Matsuhiro, Hirofumi Nakamura, T. Hayashi, Hiroo Nakamura and M. Sugimoto, Evaluation of Tritium Permeation from Lithium Loop of IFMIF Target System, Fusion Science and Technology 48 (2005) pp.625-628.

[5.3] M. Ida, H. Nakamura and M. Sugimoto, Analytical Estimation of Accessibility to the Activated Lithium Loop in IFMIF, Journal of Nuclear Materials 367-370 (2007) pp.1557-1561.

[5.4] U. von Möllendorff, F. Maekawa, H. Giese and H. Feuerstein, A nuclear simulation experiment for the International Fusion Materials Irradiation Facility (IFMIF), FZK report FZKA 6764, 2002.

[5.5] M. Baba, Experimental Studies on Particle and Radionuclide Production Cross Sections for Tens of MeV Neutrons and Protons, AIP Conference proceedings 769 (2004) p.884.

[5.6] H. Migge, Second Topical Meeting on Fusion Reactor Materials, Seattle, WA, August 9-12, 1981.

[5.7] Y. Sakamoto and S. Tanaka, QAD-CGGP2 and G33-GP2: Revised versions of QAD-CGGP and G33-GP, JAERI report JAERI-M 90-110, 1999.

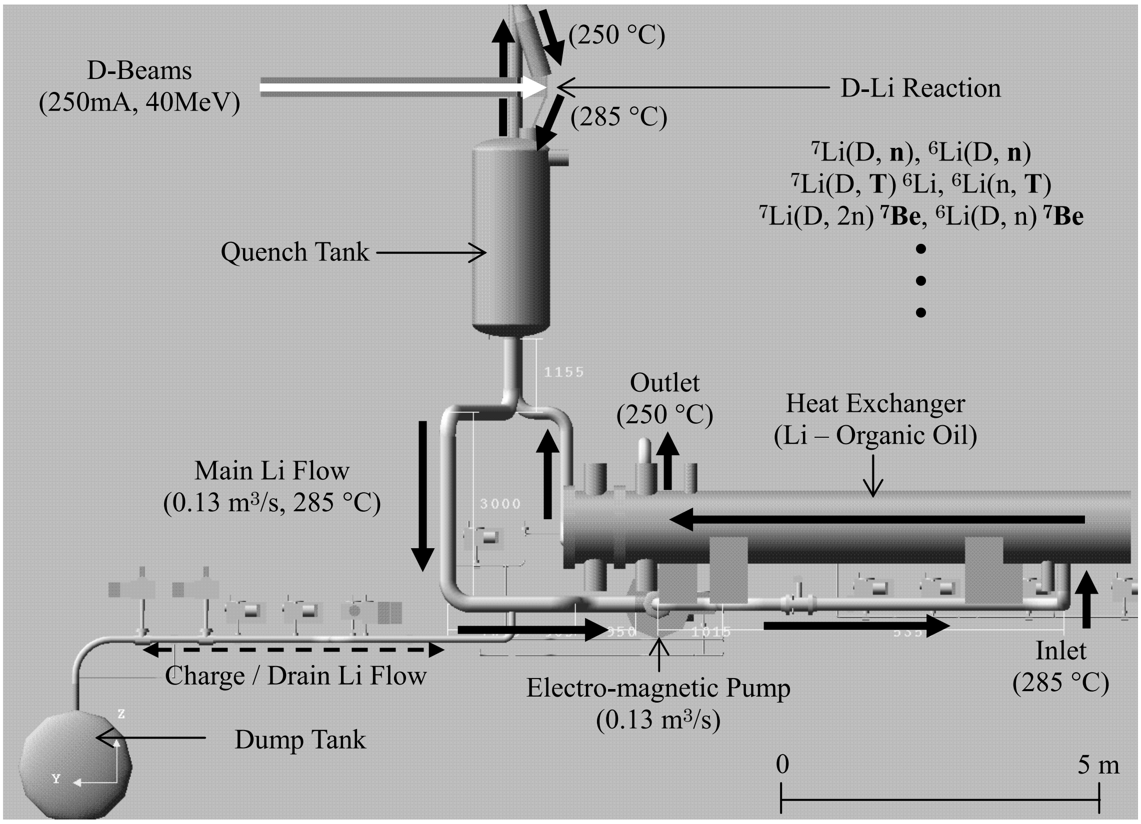

Fig. 5.1 Vertical layout of the IFMIF lithium loop

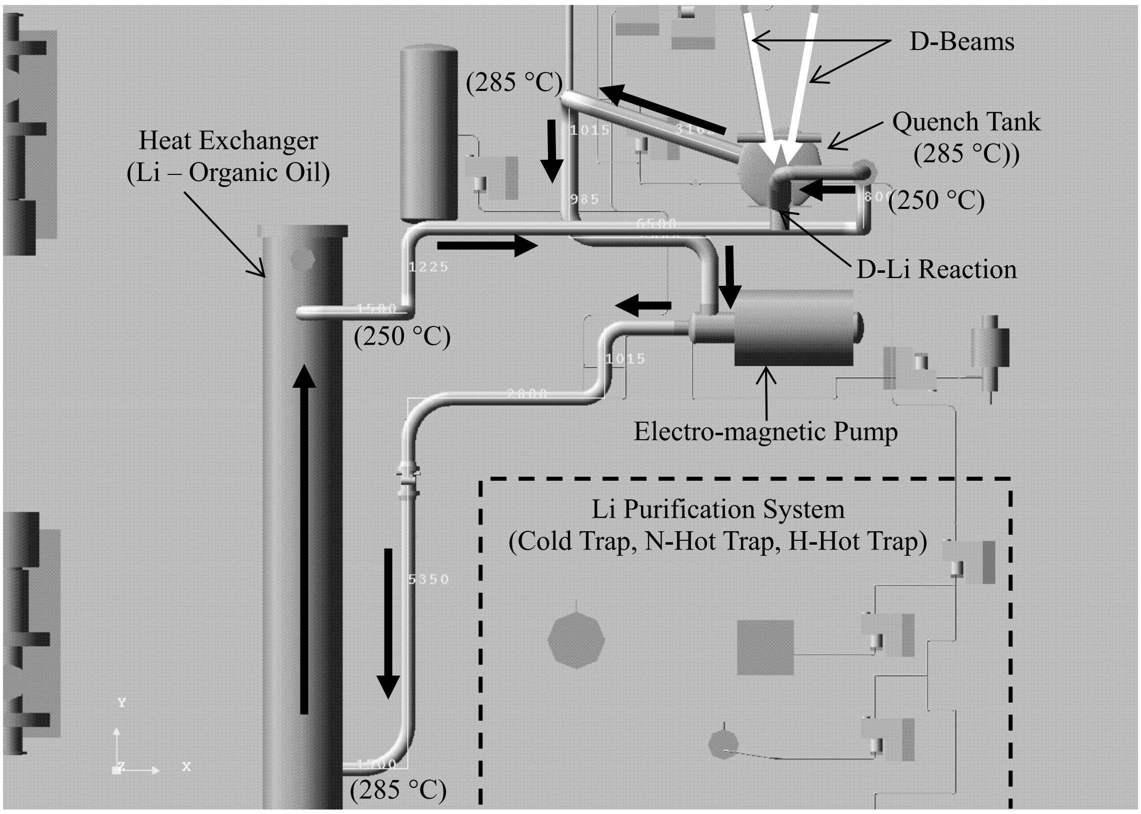

Fig. 5.2 Horizontal layout of the IFMIF lithium loop

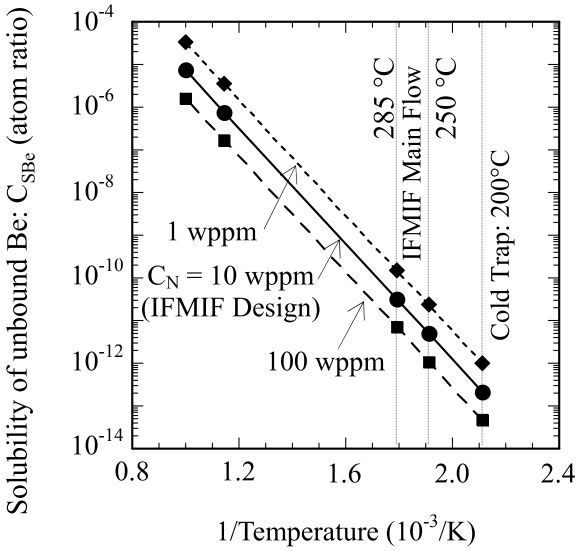

Fig. 5.3 Solubility of unbound Be in liquid Li

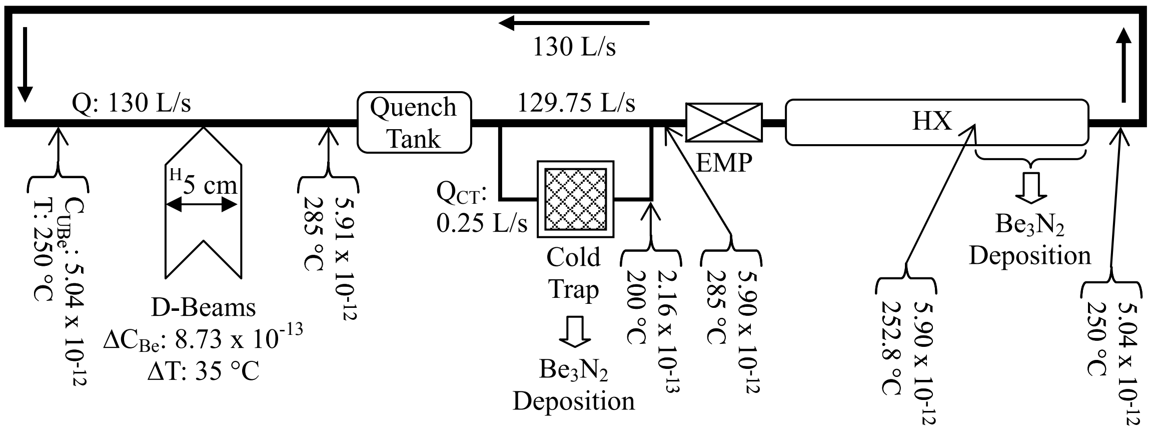

Fig. 5.4 Concentration of unbound ^{7}Be in IFMIF Li loop

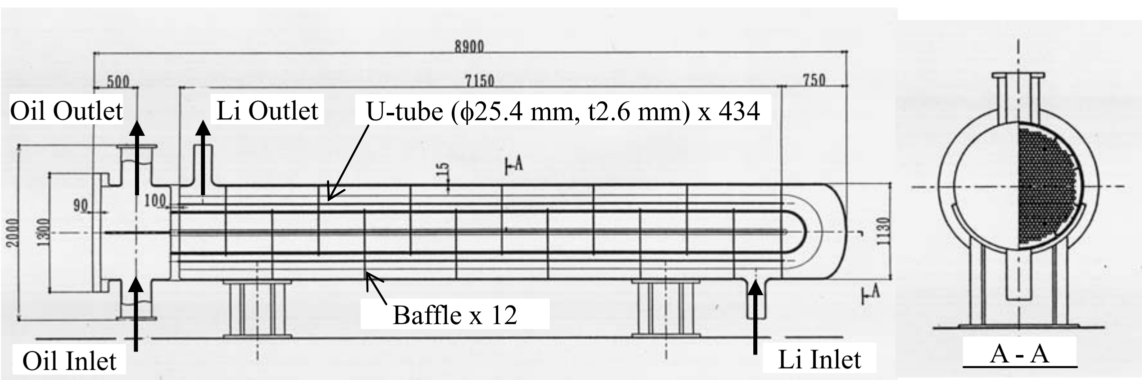

Fig. 5.5 Cross-sectional view of primary heat exchanger

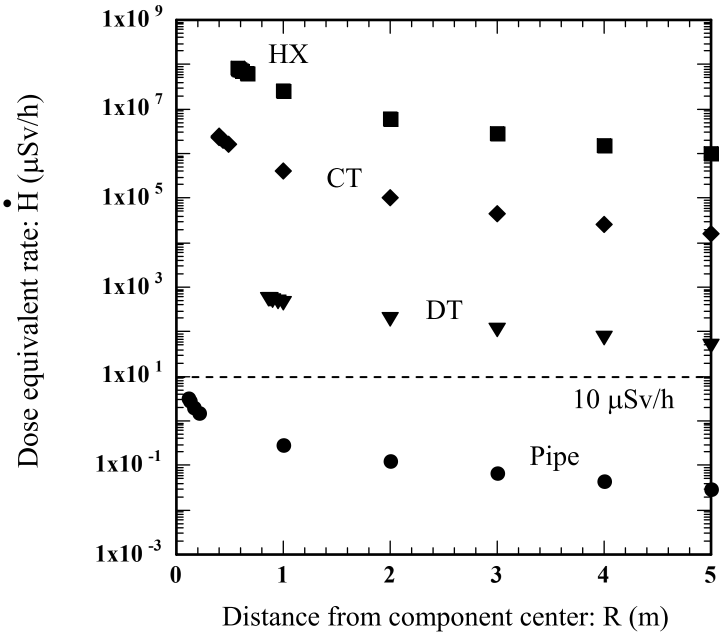

Fig. 5.6 Dose rate around components without shields (Case-1)

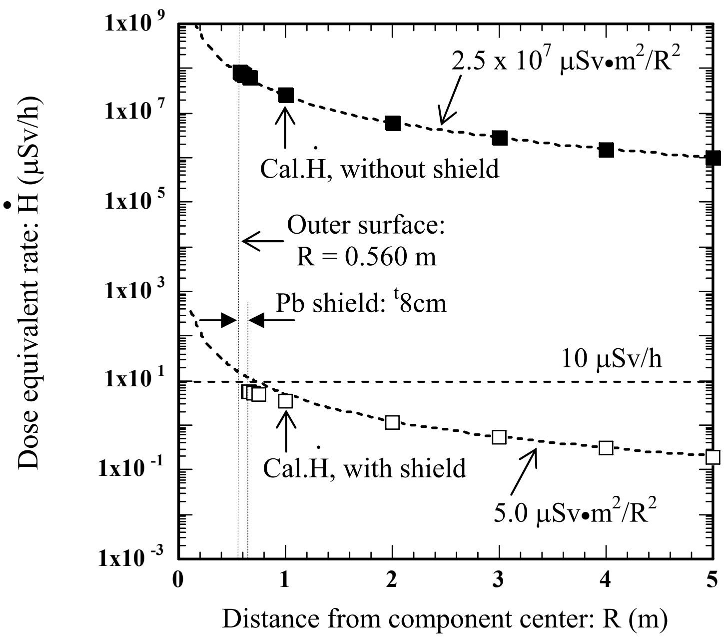

Fig. 5.7 Dose rate around heat exchanger (Case-1)

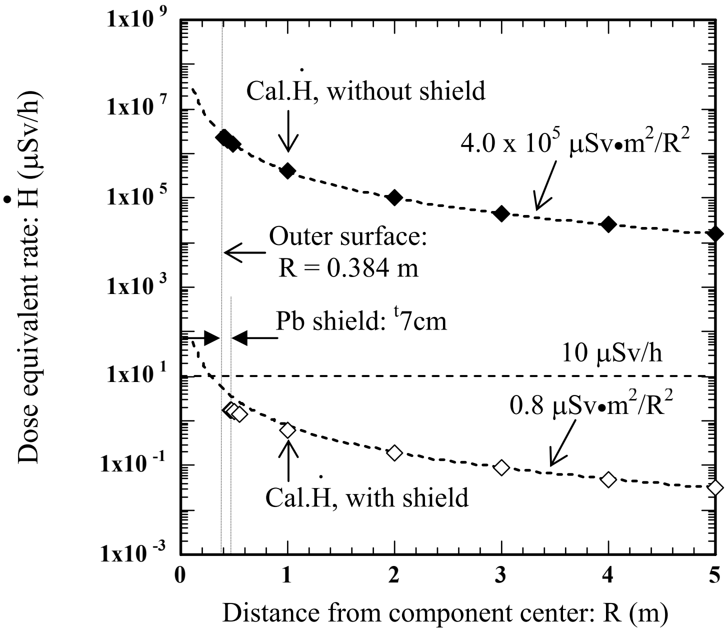

Fig. 5.8 Dose rate around cold trap (Case-1)

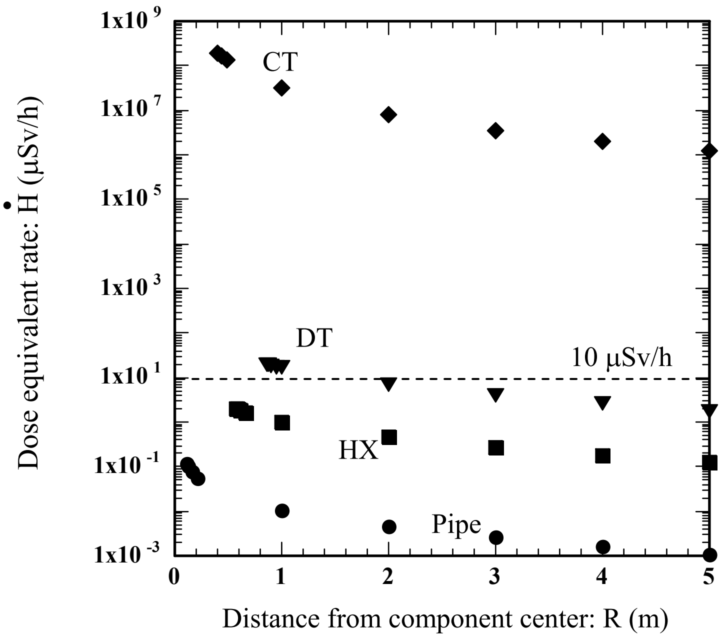

Fig. 5.9 Dose rate around components without shields (Case-2)

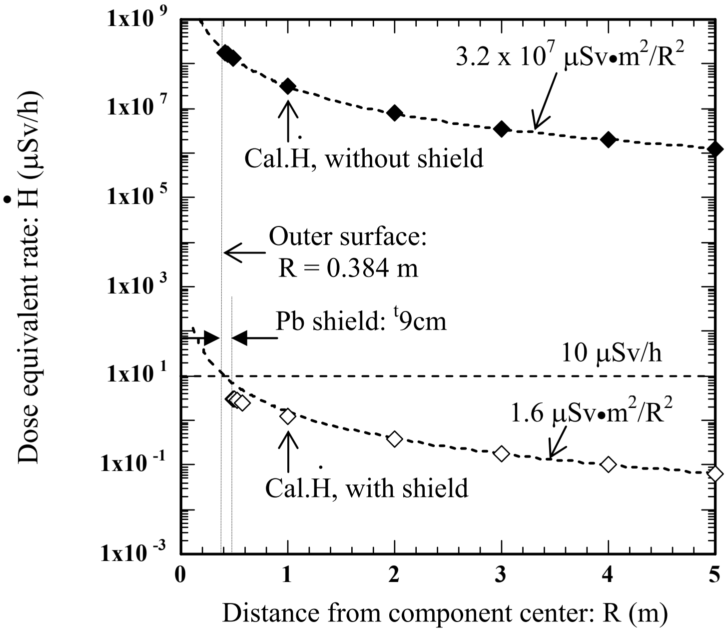

Fig. 5.10 Dose rate around cold trap (Case-2)

6. Consideration on EVEDA Tasks

6.1 EVEDA Tasks for Target Facility

IFMIF Engineering Validation and Engineering Design Activities (IFMIF-EVEDA) are to be implemented as one of three projects under the Agreement between the Government of Japan and the European Atomic Energy Community for the Joint Implementation of the Broader Approach Activities (BA) in the Field of Fusion Energy Research. The Engineering Design is completed to a level corresponding to procurement. The Engineering Validation is completed to validate safe stable operation of each system with high availability. For the target system, tasks shown in Table 6.1 shall be carried out.

Table 6.1 EVEDA task list for Target Facilities

Task Title	Brief Task Description
Construction, operation and tests of EVEDA Li Loop	• Construction of the Li loop consisting of a main loop, an electromagnetic pump, a heat exchanger, excepting diagnostics and tritium/impurity monitors and traps • Operation of Li test loop and validation of the Li loop performance in long-term operation
Erosion / Corrosion	• Erosion / corrosion measurements in material loop and EVEDA Li Loop
Diagnostics	• Li jet free surface and thickness monitor in Li test loop, distortion monitor of the target assembly, surface temperature monitor, Li vapor monitor
Li purification system	• Validation of removal and monitoring of tritium, ^{7}Be, C, N and O
Remote handling and Li safety handling	• Development and verification of remote handling system for the back-wall and target assembly • Validation of thermal and thermo-structural characteristics of the target assembly including the back-wall • Tests on Li leak, combustion, extinction, and radioactive materials behavior as aerosols for safe operation
Engineering Design	• Design of the target assembly, the Li main loop, the Li purification loop • Design of various diagnostics and arrangements • Design of the remote handling system for the target assembly and/or the back-wall • Safety analysis and design of vacuum system and control system

6.2 Construction and Operation of EVEDA Li Loop

The stability of Li flow in long-time is validated using the EVEDA Li Loop, which consists of a contraction nozzle and a concave channel hydraulically well simulating the IFMIF target flow, and a purification system to control impurity level at the IFMIF condition. Also diagnostics for the high-speed, free-surface flow and impurity traps/monitors are validated in the EVEDA Li Loop. For efficiency of these activities, supplemental tests are done by using a water loop and an existing Li loop. This task containing the activities above mentioned is the main one among the EVEDA target tasks, and requires long duration and large amount of cost. Therefore, contents of the task were investigated ahead in FY2006 as follows.

6.2.1 Construction of the EVEDA Li Loop

Design of the EVEDA Li loop with thickness of Li jet: 0.025 m, width of Li jet: 0.10 m, flow velocity of Li jet: ≤ 20 m/s and Li inventory: ~4 m^3 is done. Most of other specification is the same as that of IFMIF Li loop. Typical different points are the width of Li jet which is 1/2.6 of IFMIF Li jet, no beam injection and thus no tritium in liquid Li. Two hot-traps for N and H removal and diagnostics are proposed in other tasks. Preliminary design of the target assembly as a part of the EVEDA Li Loop is shown in Fig. 6.2. This assembly has several ports for measurement/observation/lighting. After the design, procurement for fabrication of EVEDA Li loop is done. The loop is installed in a sodium facility, JAEA Oarai site, to utilize existing utility and operational/handling skills for liquid metal.

6.2.2 Performance Tests of Loop and Main Components

Tests of the EVEDA Li Loop for basic performance such as check on safety system (Li leak, interlock, etc.); characteristic tests on control of pressure (vacuum, gas supply, etc.); characteristic tests on each component (pumps, flow-meters, valves, etc.); operational tests on startup/shutdown procedure; characteristic tests on control of flow velocity: 1-20 m/s; and characteristic tests on control of plant temperature: 200-300 °C are done.

6.2.3 Validation of Impurity Traps/Monitors on at EVEDA Li Loop

Traps and monitors such as Cold Trap, Hot Trap for control of H, Hot trap for control of N, a conductivity monitor for H+C+N+O and a permeation monitor for H for measurement of concentration of each element by off-line sampling are combined to the EVEDA Li loop and validated. The latter three are proposed in another task.

6.2.4 Validation of Diagnostics on High-speed, Free-surface Flow

Diagnostics are combined to the EVEDA Li loop and validated. Excepting conventional methods, candidate diagnostics methods to be validated are pattern projection method for steady deviation of free-surface; contact probe, ultrasonic sensor and laser reflection method for unsteady deviation of free-surface; particle image velocimetry (PIV) for free-surface velocity; and permeation method for H.

6.2.5 Validation of Operation with stable Li flow

High-speed operation at 10-20 m/s in a few thousands hours under condition of impurity control; monitoring on impurity concentration in long-time; monitoring on Li vaporization and vacuum condition in long-time; and estimation of erosion/corrosion after long-time operation are done.

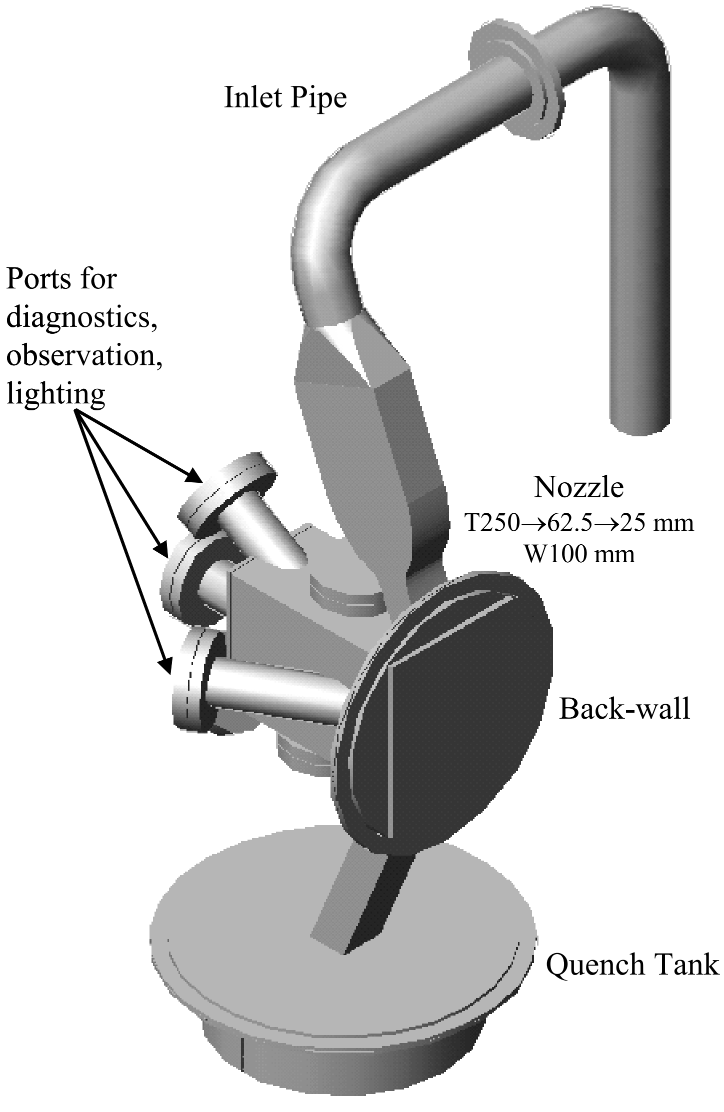

Fig. 6.1 3-D view of target assembly of the EVEDA Li Loop

6.3 Li Safety Handling

Objectives of this task are to clarify behaviors of Li leakage / combustion, and to establish suppression / extinguishment measures for assurance of safe operation of the Li loop. The contents were investigated ahead in FY2006 as follows.

6.3.1 Experiments of Li treatment

To clarify chemical reaction, experiments with parameters of Li temperature and environment, and evaluations on characteristics of reaction between Li and atmosphere gases and basic characteristics of reaction rate and temperature, etc. are done. To develop and optimize safe Li disposal management technology, characteristics of removal and cleaning of deposited Li and reaction products in maintenance and Li leakage are evaluated. To establish chemical analysis technologies, off-line analysis method of impurities in Li is tested, and the technology is validated by Li sampling at the EVEDA Li loop.

6.3.2 Experiments of Li combustion

To evaluate basic Li combustion characteristics on Li fire temperature, burning temperature, burning rate and fire without external heat source, experiments are done. To evaluate combustion characteristics of liquid Li after leakage and combustion products under air environment, to evaluate differences of combustion characteristics, and to observe corrosion of liner on floor inside experiment area Li leakage/combustion, experiment as shown in Fig. 6.2 are done.

6.3.3 Suppression and extinguishment procedures

Relating to suppression and extinguishment of Li combustion, candidate materials are compared, characteristics are evaluated, and optimal material is selected considering efficiency and maintenance (see Fig. 6.3). Relating to Li combustion, control method is considered from a view point of maintenance, arrangement of detectors and observation system for quick detection is optimized, floor liner and structure to confine Li leakage is evaluated, and efficiency of suppression and extinguishment is improved

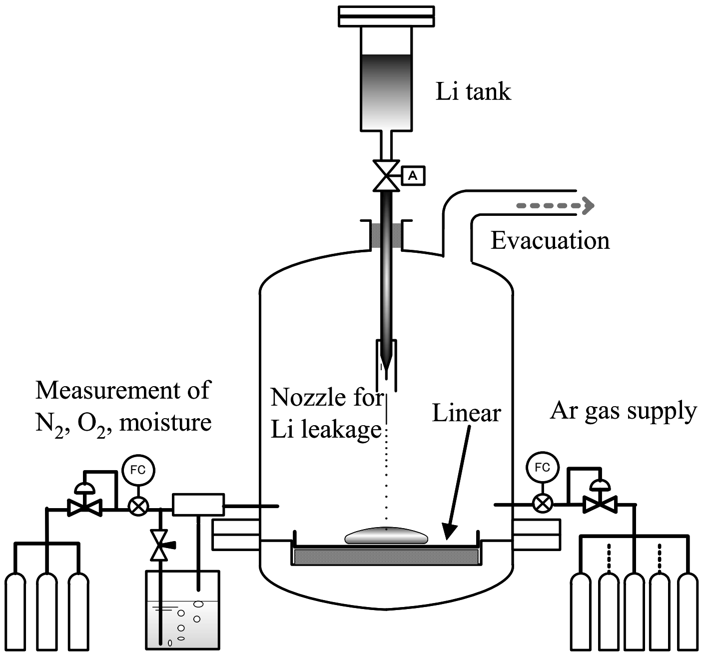

Fig. 6.2 Image of experimental set-up for Li combustion

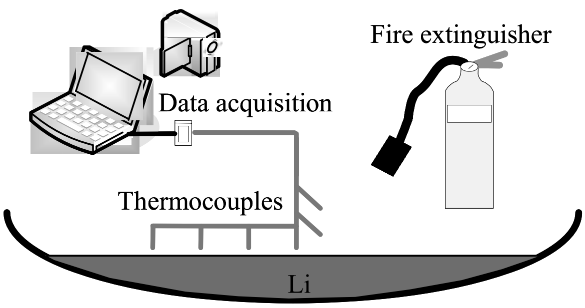

Fig. 6.3 Image of experimental set-up for extinguish performance

7. Summary

Thermo-structural analysis of the “cut and reweld” type replaceable back-wall has been carried out. A lip seal with the stress mitigation structure was proposed to reduce thermal stress. The maximum von Mises stresses of the center part of back-wall was 93 MPa, allowable for the reduced activation ferritic/martensitic steel F82H. The stress of the lip seal was 335 MPa, slightly higher than the allowable stress for the austenitic stainless steel 316L. An optimization of the 316L lip seal configuration satisfies the allowable stress criterion for the latter case.

Preliminary fabrication and tests of the weld specimens were done. Most of the weld seemed to be done successfully for both of YAG weld on 316L-316L and TIG weld on 316L-F82H. Ultimate tensile stress (UTS) of the 316L-316L specimens was less than that of non-weld specimens, and fractures occurred in their weld zone. On the contrary, UTS of the 316L-F82H specimen was roughly equal to that of non-weld specimens, and fractures occurred in the base metal of 316L. This showed integrity of the 316L-F82H weld using the filler metal Y309.

Radioactivity due to beryllium-7 (^{7}Be) deposited in typical components of the IFMIF lithium (Li) loop was estimated. Also requirement on radiation shielding was estimated. Most of ^{7}Be generated through deuteron-lithium (D-Li) reactions with rate of 5.02×10^{15} Be/s is deposited in the form of Be_3N_2 in rather cold location, such as the heat exchanger (HX) and the cold trap (CT). In case of immediate Li-drain to the dump tank after the deuteron beam stop, dose equivalent rate around HX and CT without radiation shields was respectively 8.4×10^{7} and 2.5×10^{6} μSv/h, several orders higher than a guideline of 10 μSv/h. Thickness of needed radiation shield made of lead (Pb) is 8 cm for HX and 7 cm for CT, respectively. Employment of the shutdown scheme of Li circulation with trapping by CT significantly reduces the total weight of Pb-shield from 33 tons to 4.4 tons.

Outline of EVEDA target tasks was considered, especially for the tasks carried out in mainly JAEA. The EVEDA Li target is almost equal to the IFMIF target in size excepting about 1/3 size in flow width to sufficiently simulate the IFMIF target flow. Long term hydraulic tests and validation on diagnostics and purification will be done with the EVEDA Li Loop. Li experiments for chemical reaction, combustion and fire suppression will be done in another task.

Acknowledgements

Appreciation is given to all members of the IFMIF international team on their contributions to this work. Profs. H. Matsui, T. Muroga, S. Tanaka, H. Horiike, T. Terai, S. Fukada and A. Suzuki are appreciated for their contributions on planning of EVEDA tasks. The IFMIF executive subcommittee has been highly impressed with dedication and enthusiasm of the IFMIF team. Also, appreciation is given to for the continued interest of the IEA Fusion Power Coordinating Committee and IEA Executive Committee on Fusion Material. Finally, the authors in JAEA are grateful to Drs. M. Seki, T. Tsunematsu, S. Seki, Y. Okumura, Y. Wada, H. Takatsu and T. Nishitani for their supports to IFMIF activities.

国際単位系（SI）

表１．SI 基本単位

基本量	SI 基本単位	
	名称	記号
長さ	メートル	m
質量	キログラム	kg
時間	秒	s
電流	アンペア	A
熱力学温度	ケルビン	K
物質量	モル	mol
光度	カンデラ	cd

表２．基本単位を用いて表されるSI組立単位の例

組立量	SI 基本単位	
	名称	記号
面積	平方メートル	m^2
体積	立法メートル	m^3
速さ，速度	メートル毎秒	m/s
加速度	メートル毎秒毎秒	m/s^2
波数	毎メートル	m-1
密度（質量密度）	キログラム毎立法メートル	kg/m^3
質量体積（比体積）	立法メートル毎キログラム	m^3/kg
電流密度	アンペア毎平方メートル	A/m^2
磁界の強さ	アンペア毎メートル	A/m
（物質量の）濃度	モル毎立方メートル	mol/m^3
輝度	カンデラ毎平方メートル	cd/m^2
屈折率	（数の）１	1

表５．SI 接頭語

乗数	接頭語	記号	乗数	接頭語	記号
10^{24}	ヨタ	Y	10^{-1}	デシ	d
10^{21}	ゼタ	Z	10^{-2}	センチ	c
10^{18}	エクサ	E	10^{-3}	ミリ	m
10^{15}	ペタ	P	10^{-6}	マイクロ	µ
10^{12}	テラ	T	10^{-9}	ナノ	n
10^{9}	ギガ	G	10^{-12}	ピコ	p
10^{6}	メガ	M	10^{-15}	フェムト	f
10^{3}	キロ	k	10^{-18}	アト	a
10^{2}	ヘクト	h	10^{-21}	ゼプト	z
10^{1}	デカ	da	10^{-24}	ヨクト	y

表３．固有の名称とその独自の記号で表されるSI組立単位

組立量	SI 組立単位			
	名称	記号	他のSI単位による表し方	SI基本単位による表し方
平面角	ラジアン[a]	rad		$m \cdot m^{-1}=1$[b]
立体角	ステラジアン[a]	sr[c]		$m^2 \cdot m^{-2}=1$[b]
周波数	ヘルツ	Hz		s^{-1}
力	ニュートン	N		$m \cdot kg \cdot s^{-2}$
圧力，応力	パスカル	Pa	N/m^2	$m^{-1} \cdot kg \cdot s^{-2}$
エネルギー，仕事，熱量	ジュール	J	N・m	$m^2 \cdot kg \cdot s^{-2}$
工率，放射束	ワット	W	J/s	$m^2 \cdot kg \cdot s^{-3}$
電荷，電気量	クーロン	C		s・A
電位差（電圧），起電力	ボルト	V	W/A	$m^2 \cdot kg \cdot s^{-3} \cdot A^{-1}$
静電容量	ファラド	F	C/V	$m^{-2} \cdot kg^{-1} \cdot s^4 \cdot A^2$
電気抵抗	オーム	Ω	V/A	$m^2 \cdot kg \cdot s^{-3} \cdot A^{-2}$
コンダクタンス	ジーメンス	S	A/V	$m^{-2} \cdot kg^{-1} \cdot s^3 \cdot A^2$
磁束	ウエーバ	Wb	V・s	$m^2 \cdot kg \cdot s^{-2} \cdot A^{-1}$
磁束密度	テスラ	T	Wb/m^2	$kg \cdot s^{-2} \cdot A^{-1}$
インダクタンス	ヘンリー	H	Wb/A	$m^2 \cdot kg \cdot s^{-2} \cdot A^{-2}$
セルシウス温度	セルシウス度[d]	℃		K
光束	ルーメン	lm	cd・sr[c]	$m^2 \cdot m^{-2} \cdot cd=cd$
照度	ルクス	lx	lm/m^2	$m^2 \cdot m^{-4} \cdot cd=m^{-2} \cdot cd$
（放射性核種の）放射能	ベクレル	Bq		s^{-1}
吸収線量，質量エネルギー分与，カーマ	グレイ	Gy	J/kg	$m^2 \cdot s^{-2}$
線量当量，周辺線量当量，方向性線量当量，個人線量当量，組織線量当	シーベルト	Sv	J/kg	$m^2 \cdot s^{-2}$

(a)ラジアン及びステラジアンの使用は、同じ次元であっても異なった性質をもった量を区別するときの組立単位の表し方として利点がある。組立単位を形作るときのいくつかの用例は表４に示されている。
(b)実際には、使用する時には記号rad及びsrが用いられるが、習慣として組立単位としての記号“１”は明示されない。
(c)測光学では、ステラジアンの名称と記号srを単位の表し方の中にそのまま維持している。
(d)この単位は、例としてミリセルシウス度m℃のようにSI接頭語を伴って用いても良い。

表４．単位の中に固有の名称とその独自の記号を含むSI組立単位の例

組立量	SI 組立単位		
	名称	記号	SI 基本単位による表し方
粘度	パスカル秒	Pa・s	$m^{-1} \cdot kg \cdot s^{-1}$
力のモーメント	ニュートンメートル	N・m	$m^2 \cdot kg \cdot s^{-2}$
表面張力	ニュートン毎メートル	N/m	$kg \cdot s^{-2}$
角速度	ラジアン毎秒	rad/s	$m \cdot m^{-1} \cdot s^{-1}=s^{-1}$
角加速度	ラジアン毎平方秒	rad/s^2	$m \cdot m^{-1} \cdot s^{-2}=s^{-2}$
熱流密度，放射照度	ワット毎平方メートル	W/m^2	$kg \cdot s^{-3}$
熱容量，エントロピー	ジュール毎ケルビン	J/K	$m^2 \cdot kg \cdot s^{-2} \cdot K^{-1}$
質量熱容量（比熱容量），質量エントロピー	ジュール毎キログラム毎ケルビン	J/(kg・K)	$m^2 \cdot s^{-2} \cdot K^{-1}$
質量エネルギー（比エネルギー）	ジュール毎キログラム	J/kg	$m^2 \cdot s^{-2} \cdot K^{-1}$
熱伝導率	ワット毎メートル毎ケルビン	W/(m・K)	$m \cdot kg \cdot s^{-3} \cdot K^{-1}$
体積エネルギー	ジュール毎立方メートル	J/m^3	$m^{-1} \cdot kg \cdot s^{-2}$
電界の強さ	ボルト毎メートル	V/m	$m \cdot kg \cdot s^{-3} \cdot A^{-1}$
体積電荷	クーロン毎立方メートル	C/m^3	$m^{-3} \cdot s \cdot A$
電気変位	クーロン毎平方メートル	C/m^2	$m^{-2} \cdot s \cdot A$
誘電率	ファラド毎メートル	F/m	$m^{-3} \cdot kg^{-1} \cdot s^4 \cdot A^2$
透磁率	ヘンリー毎メートル	H/m	$m \cdot kg \cdot s^{-2} \cdot A^{-2}$
モルエネルギー	ジュール毎モル	J/mol	$m^2 \cdot kg \cdot s^{-2} \cdot mol^{-1}$
モルエントロピー，モル熱容量	ジュール毎モル毎ケルビン	J/(mol・K)	$m^2 \cdot kg \cdot s^{-2} \cdot K^{-1} \cdot mol^{-1}$
照射線量（Ｘ線及びγ線）	クーロン毎キログラム	C/kg	$kg^{-1} \cdot s \cdot A$
吸収線量率	グレイ毎秒	Gy/s	$m^2 \cdot s^{-3}$
放射強度	ワット毎ステラジアン	W/sr	$m^4 \cdot m^{-2} \cdot kg \cdot s^{-3}=m^2 \cdot kg \cdot s^{-3}$
放射輝度	ワット毎平方メートル毎ステラジアン	$W/(m^2 \cdot sr)$	$m^2 \cdot m^{-2} \cdot kg \cdot s^{-3}=kg \cdot s^{-3}$

表６．国際単位系と併用されるが国際単位系に属さない単位

名称	記号	SI 単位による値
分	min	1 min=60s
時	h	1h =60 min=3600 s
日	d	1 d=24 h=86400 s
度	°	1°=(π/180) rad
分	’	1’=(1/60)°=(π/10800) rad
秒	”	1”=(1/60)’=(π/648000) rad
リットル	l、L	1l=1 $dm^3=10^{-3}m^3$
トン	t	1t=10^3 kg
ネーパ	Np	1Np=1
ベル	B	1B=(1/2)ln10(Np)

表７．国際単位系と併用されこれに属さない単位で
SI単位で表される数値が実験的に得られるもの

名称	記号	SI 単位であらわされる数値
電子ボルト	eV	1eV=1.60217733(49)×10^{-19}J
統一原子質量単位	u	1u=1.6605402(10)×10^{-27}kg
天文単位	ua	1ua=1.49597870691(30)×10^{11}m

表８．国際単位系に属さないが国際単位系と
併用されるその他の単位

名称	記号	SI 単位であらわされる数値
海里		1海里=1852m
ノット		1ノット=1海里毎時=(1852/3600)m/s
アール	a	1 a=1 $dam^2=10^2m^2$
ヘクタール	ha	1 ha=1 $hm^2=10^4m^2$
バール	bar	1 bar=0.1MPa=100kPa=1000hPa=10^5Pa
オングストローム	Å	1 Å=0.1nm=10^{-10}m
バーン	b	1 b=100$fm^2=10^{-28}m^2$

表９．固有の名称を含むCGS組立単位

名称	記号	SI 単位であらわされる数値
エルグ	erg	1 erg=10^{-7} J
ダイン	dyn	1 dyn=10^{-5}N
ポアズ	P	1 P=1 dyn・s/cm^2=0.1Pa・s
ストークス	St	1 St =1cm^2/s=$10^{-4}m^2$/s
ガウス	G	1 G [illegible]10^{-4}T
エルステッド	Oe	1 Oe [illegible](1000/4π)A/m
マクスウェル	Mx	1 Mx [illegible]10^{-8}Wb
スチルブ	sb	1 sb =1cd/cm^2=10^4cd/m^2
ホト	ph	1 ph=10^4lx
ガル	Gal	1 Gal =1cm/s^2=10^{-2}m/s^2

表10．国際単位に属さないその他の単位の例

名称	記号	SI 単位であらわされる数値
キュリー	Ci	1 Ci=3.7×10^{10}Bq
レントゲン	R	1 R = 2.58×10^{-4}C/kg
ラド	rad	1 rad=1cGy=10^{-2}Gy
レム	rem	1 rem=1 cSv=10^{-2}Sv
X線単位		1X unit=1.002×10^{-4}nm
ガンマ	γ	1γ=1 nT=10^{-9}T
ジャンスキー	Jy	1 Jy=10^{-26}W・m^{-2}・Hz^{-1}
フェルミ		1 fermi=1 fm=10^{-15}m
メートル系カラット		1 metric carat = 200 mg = 2×10^{-4}kg
トル	Torr	1 Torr = (101 325/760) Pa
標準大気圧	atm	1 atm = 101 325 Pa
カロリー	cal	
ミクロン	µ	1 µ =1µm=10^{-6}m

（第７版，1998年改訂）